# Energetics of Quinone−Dependent Electron and Proton Transfers in Rhodobacter spheroides, Photosynthetic Reaction Centers

**ARTICLE** *in* BIOCHEMISTRY · FEBRUARY 2005

Impact Factor: 3.02 · DOI: 10.1021/bi048348k · Source: PubMed

# Energetics of Quinone-Dependent Electron and Proton Transfers in *Rhodobacter sphaeroides* Photosynthetic Reaction Centers

Zhenyu Zhu and M. R. Gunner*

*Physics Department J-419, City College of New York, 138th Street and Convent Avenue, New York, New York 10031*

*Received August 2, 2004; Revised Manuscript Received September 23, 2004*

ABSTRACT: Proteins bind redox cofactors, modifying their electrochemistry and affinity by specific interactions of the binding site with each cofactor redox state. Photosynthetic reaction centers from *Rhodobacter sphaeroides* have three ubiquinone-binding sites, $Q_A$, and proximal and distal $Q_B$ sites. Ubiquinones, which can be doubly reduced and bind 2 protons, have 9 redox states. However, only Q and $Q^-$ are seen in the $Q_A$ site and Q, $Q^-$, and $QH_2$ in the proximal $Q_B$ site. The distal $Q_B$ function is uncertain. Multiple conformation continuum electrostatics (MCCE) was used to compare the ubiquinone electrochemical midpoints ($E_m$) and p$K_a$ values at these three sites. At pH 7, the $Q_A/Q_A^-$ $E_m$ is −40 mV and proximal $Q_B/Q_B^-$ −10 mV in agreement with the experimental values (assuming a solution ubiquinone $E_m$ of −145 mV). $Q_B$ reduction requires changes in nearby residue protonation and SerL223 reorientation. The distal $Q_B/Q_B^-$ $E_m$ is a much more unfavorable −260 mV. $Q_A$ and proximal $Q_B$ sites generally stabilize species with a −1 charge, while the distal $Q_B$ site prefers binding neutral species. In each site, the dianion is destabilized because favorable interactions with the residues and backbone increase with charge ($q$), while the unfavorable loss of solvation energy increases with $q^2$. Therefore, proton binding before a second reduction, forming QH and then $QH^-$, is always preferred to forming the dianion ($Q^{-2}$). The final product $QH_2$ is higher in energy at the proximal $Q_B$ site than in solution; therefore, it binds poorly, favoring release. In contrast, $QH_2$ binds more tightly than Q at the distal $Q_B$ site.

Quinones are found in many transmembrane proteins that coupled electron and proton transfer reactions (*1*, *2*), including photosynthetic reaction centers, PSII (*3*), PSI (*4*), cytochrome $bc_1$ (*5*), and $b_6f$ complexes (*6*−*8*), and in the quinol:fumarate (*9*) and succinate:quinone (*10*) oxidoreductases. With their ability to bind 2 protons and 2 electrons, quinones have 9 redox states (Figure 1) (*11*). In aqueous solution at physiological pH, these quinones go from being fully oxidized (Q) to fully reduced ($QH_2$) in a concerted two electron and two proton reaction (*11*). This electrochemistry is modified within individual proteins; therefore, reactions can proceed via single electron transfers so reduction steps do not need to be coupled to proton uptake.

The quinone-dependent electron and proton transfers in bacterial reaction centers (RCs) of *Rhodobacter sphaeroides* have been well-studied (*1*, *2*, *12*), providing a wealth of information that can be subjected to computational analysis (*13*). This theoretical analysis enhances our understanding of the protein while providing good tests of evolving computational methods. RCs consist of three protein subunits, L, M, and H, and 10 cofactors including 2 ubiquinones. The intraprotein electron transfer occurs along the L branch from the excited singlet bacteriochlorophyll dimer (P), through a bacteriochlorophyll monomer (B) and bacteriopheophytin monomer (H) to the primary quinone $Q_A \approx 25$ Å away in 150 ps. $Q_A$ then reduces the secondary quinone $Q_B$ 15 Å away (edge to edge) in 100 $\mu$s (*14*, *15*). Cytochrome *c* reduces $P^+$, yielding $PQ_AQ_B^-$. After a second excitation of P, $P^+Q_A^-Q_B^-$ is formed. There is good evidence that $Q_B$ binds a proton (forming $Q_BH$) prior to its second reduction (*16*). The second reduction of $Q_B$ then forms $Q_BH^-$, which binds a second proton, yielding the dihydroquinone. Overall, two cycles of light-driven reactions oxidize two cytochromes c in the periplasm, delivering these two electrons along with two protons from the cytoplasm to $Q_B$. The reduced dihydroubiquinone is released to the cell membrane, and a new oxidized quinone is bound (*17*). In the cell, electron transfer from the dihydroquinone back to cytochrome *c* occurs in the cytochrome $bc_1$ complex, which adds to the transmembrane proton gradient by releasing protons into the periplasm.

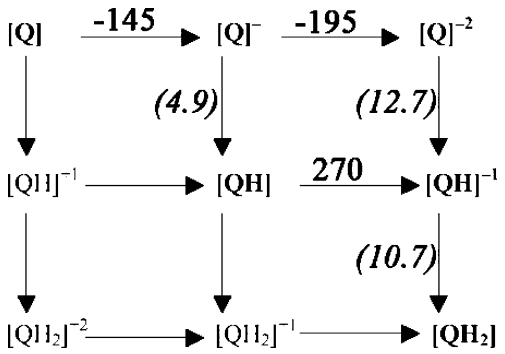


FIGURE 1: Ubiquinone redox and protonation states. States in bold are intermediates considered in coupled electron (horizontal) and proton (vertical) transfer reactions in RCs. The sources for the $E_{m,sol}$ and p$K_{a,sol}$ (in parentheses) at pH 7 are given in Table 1. The $\Delta G$ for proton transfer (vertical lines) can be obtained from $\Delta G = 59.3\text{-}(pH - pK_a)$ (eq 9).

* To whom correspondence should be addressed. Telephone: 212-650-5557. Fax: 212-650-6940. E-mail: gunner@sci.ccny.cuny.edu.

10.1021/bi048348k CCC: $30.25 
Published on Web 12/08/2004

The protein modifies the ubiquinone electrochemistry to differentiate $Q_A$ and $Q_B$. In the $Q_A$ site, only the oxidized $Q_A$ and anionic semiquinone $Q_A^-$ are found. $Q_A$ does not dissociate from the protein. $Q_B$ displays more complex redox chemistry, serving as the two-electron gate (*18*). Thus, two single electron transfers via $Q_A$ form the doubly reduced $Q_B$ for release into the membrane (*12*). RCs can be found with $Q_B$ in three relatively stable redox states: unreduced quinone (Q), anionic semiquinone ($Q^-$), and fully reduced and protonated dihydroquinone ($QH_2$). The anionic semiquinone is tightly bound to the protein, while the Q and $QH_2$ freely exchange with the quinone pool in the membrane (*19*). The pathway for the second reduction indicates that of the two possible intermediates $Q_BH$ is easier to form than $Q_B^{-2}$; therefore, proton binding occurs prior to electron transfer. Thus, of the nine possible redox states for $Q_B$, five are found on the reaction pathway (Figure 1). In addition, in the reaction scheme, it is necessary that the redox potentials of $Q_B$ for the first and second reduction are maintained so that $Q_A^-$ can reduce both $Q_B$ and $Q_BH$. Lastly, there are two binding sites for $Q_B$, distal and proximal, seen in the crystal structures (*20*, *21*). Kinetic measurements find no evidence for quinone reduction in the outer, distal site (*22*−*26*), although this has been proposed by simulation (*27*). A comparison of the thermodynamics of quinone reduction in the two sites can help to determine what redox states are accessible in the distal site.

The different *in situ* thermodynamic properties of $Q_A$ and $Q_B$ can be attributed to different local environments. $Q_B$ is surround by a cluster of polar residues, acids, and waters, including SerL223, AspL210, GluL212, AspL213, GluH173, AsnM44, and AspM17. These residues have been identified as important for electron and proton transfer by both mutation experiments (*28*−*36*) and simulations (*37*, *38*). These residues rearrange to stabilize the anionic semiquinone and provide a pathway for proton delivery prior to and following the second reduction of $Q_B$. This flexible polar region of the protein maintains the appropriate energies of the different $Q_B$ redox states. In contrast, there are fewer ionization shifts and no proton pathway associated with reduction of $Q_A$.

With the wealth of experimental information about the redox chemistry in wild-type and mutant protein, RCs provide an excellent system to test simulation techniques. Molecular dynamics (MD) has been used to study $Q_B$ movements (*39*), conformational gating (*40*), and changes in protonation states of amino acids GluL212 and AspL213 on the first electron transfer (*41*). Continuum electrostatics (CE) simulations provide rapid estimates of long-range electrostatic interactions by averaging many motions into the dielectric constant (*13*, *42*). The first electron transfer from $Q_A^-$ to $Q_B$ has been studied by various CE methods using both *Rhodopseudomonas viridis* (*43*, *44*) and *Rb. sphaeroides* RC structures (*37*, *38*, *45*−*47*). The energetics of the second $Q_B$ reduction has also been calculated by Knapp and coworkers with a CE model in *Rps. viridis* (*44*) and *Rb. sphaeroides* (*46*) RCs.

Standard CE techniques provide two types of response to changes in charge caused by reactions such as quinone reduction (*13*, *42*, *48*). One is a homogeneous dielectric response defined by the dielectric constant used in the calculation. Values from 4 to 20 have been used with the higher values averaging more conformational changes in the protein. The other is the changes in protonation of surrounding residues. These proton shifts coupled to electron transfer are analyzed using standard methods to calculate residue p$K_a$ values (*48*−*50*). Here, no explicit conformational changes are allowed. Multiple conformation continuum electrostatics (MCCE) calculations add side-chain heavy atom and hydroxyl conformers to improve the flexibility of the CE model (*51*−*54*). This method can follow linked conformational and ionization state changes during the reduction of quinone. The work presented here uses MCCE to analyze the energies of the redox states in the $Q_A$ and distal and proximal $Q_B$ sites to determine how the protein stabilizes the appropriate states in each binding site.

## MATERIALS AND METHODS

*MCCE Methods.* MCCE (*13*, *37*, *53*, *54*) calculates the equilibrium distribution of conformation and ionization states of protein side chains, buried waters, ions, and ligands at a defined solution pH and $E_h$. Preselected choices for atomic coordinates and ionization states are used. Side-chain conformers are added providing alternative positions of hydroxyl protons of Ser, Tyr, Thr, and water, His tautomers, and the different ionization states of the acids Asp, Glu, and Tyr and the bases Arg, Lys, and His. There are at least two $Q_B$-binding sites (*20*), characterized in a comparison of protein frozen in the light (1AIG) and dark (1AIJ) (*21*, *55*). The protein structure (1AIJ) with a resolution of 2.2 Å used in this calculation has the quinone in the distal position. The proximal $Q_B$ position of 1AIG was added into the 1AIJ structure by superimposing the $Q_B$ ring, non-heme iron, and the backbone atoms of GluL212 and AspL213. Conformers of protonated quinone species are generated with 2 different hydrogen positions for each carbonyl oxygen in the plane of the quinone ring with an angle of 60° between them (Figure 5). This generates 4 neutral semiquinone (QH) and 4 dihydroquinone ($QH_2$) conformers.

Lipid and detergent molecules are removed from the structure. The 110 waters with <10 Å exposed surface area defined by SURFV (*56*, *57*) are included. Conflicts between waters at nearby positions in a given site are avoided by providing each water with a conformer that does not interact with the protein. Thus, each water molecule is allowed to leave the protein during Monte Carlo sampling. Hartree−Fock partial charges are used for each ubiquinone redox state (*44*). A +2 charge is placed on the non-heme iron between $Q_A$ and $Q_B$. The partial charges for all other cofactors are from ref *58*. PARSE partial charges and radii (*59*) are used for all other groups. For calculations involving $Q_A$ or proximal $Q_B$, no quinone conformers are allowed in the distal $Q_B$ site ($Q_{BD}$). For analysis of $Q_{BD}$, the proximal $Q_B$ site is kept unoccupied. For states where the quinone is protonated, conformers with different proton positions are allowed and their occupancy is summed. Unless otherwise noted, $Q_A$ is fixed in the oxidized state for all $Q_B$ titrations, and likewise, the proximal $Q_B$ is fixed in the quinone state and $Q_{BD}$ is deleted, for $Q_A$ titrations.

Look-up tables are calculated for electrostatic and nonelectrostatic conformer self- and conformer−conformer pairwise interactions. The electrostatic pairwise interactions and reaction field energies are calculated using the finite-difference technique to solve the Poisson−Boltzmann equa-

tion with DelPhi (*57*, *60*, *61*). Three focusing runs are done, giving a final resolution of 1.2 grids/Å (*62*). The protein is surrounded by water. The protein dielectric constant is 4, while 80 is used for the solvent with a salt concentration of 150 mM. The Lennard−Jones interactions are calculated using A and B parameters previously described (*37*). The possible microstates of the system are subjected to Monte Carlo sampling. A microstate is made up of one conformer for each residue, cofactor, and water. The energy of microstate $n$ ($\Delta G^n$)[1] is the sum of the electrostatic and nonelectrostatic energies (*63*) (eq 1). where $k_bT$ is 0.59 kcal/

$$\Delta G^n = \sum_{i=1}^{M} \delta_x(i)\{\gamma(i)[2.3k_bT(\mathrm{pH} - \mathrm{p}K_{\mathrm{sol},i}) - nF(E_h - E_{\mathrm{m,sol},i})] + (\Delta\Delta G_{\mathrm{rxn},i} + \Delta G_{\mathrm{pol},i} + \Delta G_{\mathrm{nonel},i})\} + \sum_{i=1}^{M}\delta_x(i)\sum_{j=i+1}^{M}\delta_x(j)[\Delta G_{ij}^{\mathrm{el}} + \Delta G_{ij}^{\mathrm{nonel}}] \quad (1)$$

mol (25.8 meV), $M$ is the number of conformers, $\delta_x(i)$ is 1 for conformers that are present in the state and 0 for all others, $\gamma(i)$ is 1 for bases, −1 for acids, and 0 for polar groups and waters, $n$ is the number of electrons gained or lost in redox reactions, $F$ is the Faraday constant, $\mathrm{p}K_{\mathrm{sol},i}$ is the $\mathrm{p}K_a$ of the $i$th group in solution, $E_{\mathrm{m,sol},i}$ is the midpoint potential of the $i$th cofactor in solution, $\Delta\Delta G_{\mathrm{rxn},i}$ is the difference between the conformer reaction field energy in solution and the protein (the desolvation energy), $\Delta G_{\mathrm{pol},i}$ is the pairwise electrostatic interaction of a conformer with the backbone and with side chains that have no conformational degrees of freedom, $\Delta G_{\mathrm{nonel},i}$ is the Lennard−Jones interactions with the backbone and with all side chains with no degrees of freedom plus the torsion angle energy, and $\Delta G_{ij}^{\mathrm{el}}$ and $\Delta G_{ij}^{\mathrm{nonel}}$ are the electrostatic and Lennard−Jones pairwise interactions between each conformer in the microstate. The limits on the summation of the interconformer terms ensure that each interaction is counted once. Monte Carlo sampling establishes the Boltzmann distribution of different conformers of each residue at 25 °C, providing the probabilities of the quinone reactant and product states at a given solution redox potential ($E_h$) and pH. Multiflip (*64*) between closely coupled residues is implemented (*65*). The SOFT function is not used (*54*). A total of 40 million steps of Monte Carlo sampling leads to convergence for the system with 449 residues, including waters, with conformational degrees of freedom. There are 3833 conformers to be sampled. For each reported $E_m$, three Monte Carlo runs were made and the results were averaged. The average uncertainty in the conformer occupancy is ±0.04. The uncertainty of calculated $E_m$ values is ±4 mV.

*Redox Potentials and p$K_a$ Values of Quinones in Solution.* MCCE calculates the shift in free energy of a site redox or protonation reaction when it is moved from water into the protein, providing the changes in the electrochemical midpoint, $E_m$, or $\mathrm{p}K_a$. Given a reference, $E_{\mathrm{m,sol}}$ or $\mathrm{p}K_{\mathrm{a,sol}}$ for the cofactor in solution, measurable $E_m$ and $\mathrm{p}K_a$ values in the protein can be calculated (*63*). The redox midpoint potential of $UQ/UQ^-$ and $UQ^-/UQ^{-2}$ cannot be measured in aqueous solution at pH 7 because the $E_{\mathrm{m,sol}}$ for quinone reduction to the semiquinone is lower than that for formation of the fully protonated dihydroquinone ($QH_2$). Thus, in water at physiological pH, UQ is reduced in an $n = 2$ reaction to $QH_2$ (*11*, *66*). Measurements of the one electron reactions have been made for a small number of quinones in water (*67*). In the absence of protons, the semiquinone is stable; therefore, $E_m$ measurements are far more straightforward. $E_m$ values for $Q/Q^-$ have been determined in the aprotic solvent dimethylformamide (DMF) for a large number of quinones (*68*).

Several of the aqueous $E_{\mathrm{m,sol}}$ for ubiquinones used here were estimated by comparison with the $E_m$ values of tri- and tetramethyl benzoquinones. UQ, a 2,3-dimethoxy-5-methyl-6-isoprenyl benzoquinone, is considered to behave more like trimethyl- than tetramethyl benzoquionone because the 2,3-methoxys cannot both lie in the plane of the ring. Therefore, while two adjacent methyl groups can be electron-donating into the ring, two methoxy group cannot be (*68*). In DMF, trimethyl benzoquinone has an $E_m$ for the half-reaction $Q + e^- \rightarrow Q^-$ that is 30 mV more negative than UQ, while that of the tetramethyl compound is 150 mV lower. The $E_m$ for the trimethyl semiquinone is −170 mV in water (*67*). An $E_{\mathrm{m,sol}}$ for UQ of −145 mV, 30 mV more positive than trimethyl benzoquinone, will be used here.

The $E_m$ ($Q/Q^-$) for ubiquinone in DMF was measured to be −360 mV (*68*). The value of −145 mV represents a shift of 215 mV moving from water to DMF as found for many small quinones (*69*). A pure CE analysis of the change in the Born reaction field energy on moving the Q to $Q^-$ reaction from DMF ($\epsilon = 37$) to water ($\epsilon = 80$) only predicts a shift stabilizing the anionic semiquinone by ≈40 meV, shifting the $E_{\mathrm{m,sol}}$ to −320 mV (*44*). Thus, more specific interactions of water with the semiquinone not considered in the CE analysis are assumed to shift the $E_m$ up to −145.

The aqueous $\mathrm{p}K_{\mathrm{a,sol}}$ of semiubiquinone ($UQ^-/UQH$) was estimated to be 4.9 (*67*). Higher values of 6.5 are found in 80% ethanol/water (w/w) (*70*, *71*). The $\mathrm{p}K_a$ ($QH^-/QH_2$) of UQ was measured as 13.3 in 80% ethanol/water (w/w) (*70*). Using one suggested correction of −1.6 pH units moving from 80% ethanol to water places the ubiquinone $\mathrm{p}K_{\mathrm{a,sol}}$ at ≈11.7, a high value given the electronegativity of the methoxy substitutents. Rather, the aqueous, high pH trimethyl benzoquinone $\mathrm{p}K_{\mathrm{a,sol}}$ of 10.7 will be used here (*72*). The gap between $\mathrm{p}K_{\mathrm{a,sol}}$ ($QH^-/QH_2$) and $\mathrm{p}K_{\mathrm{a,sol}}$ ($Q^{-2}/QH^-$) is rather constant at ∼1.5−2 units (*71*, *72*). This places the $\mathrm{p}K_{\mathrm{a.sol}}$ ($Q^{2-}/QH^-$) at 12.7 (*69*). Combining these $\mathrm{p}K_a$ values and the $E_{m,7}$ for $Q^- + e^- + 2H^+ \rightarrow QH_2$ of −360 mV (*69*) provides enough information to derive an $E_{\mathrm{m,sol}}$ for $Q^- + e^- \rightarrow Q^{-2}$ of −195 mV as well as the other values in Table 1. The $E_m$ ($Q^-/Q^{-2}$) for $UQ_0$ in DMF is −1080 mV (*68*, *69*).

*Calculation of the Free Energy of Quinone Reduction Reactions.* The free energy of quinone reduction or protonation reactions in RCs, $\Delta G$, at a given pH and $E_h$ is

$$\Delta G = 2.3mk_bT(\mathrm{pH} - \mathrm{p}K_a) - nF(E_h - E_m) = -2.3k_bT\log\frac{[P]}{[R]} \quad (2)$$

where $F$ is the Faraday constant, $m$ and $n$ are the number of

[1] Abbreviations: All free-energy terms $\Delta G$ and electrochemical midpoints ($E_m$) refer to standard conditions at pH 7 ($\Delta G^{\circ\prime}$ and $E_{m,7}{}^{\circ\prime}$). The energy to change a $\mathrm{p}K_a$ by 1 pH unit at 20 °C is 1.36 kcal/mol = 59.3 meV. $\mathrm{p}K_a'$ is the $\mathrm{p}K_a$ calculated from the free energy of protonation at pH 7.

Table 1: Reference $E_m$ and p$K_a$ Values for Ubiquinone 10

| half-reactions | p$K_{a,sol}$ | $E^{\circ}_{m,sol,7}$ (mV) | $\Delta G_{sol}$[a] (meV) |
|---|---|---|---|
| $Q + e^- \rightarrow Q^-$ | | −145[b] | 145 |
| $Q + 2e^- \rightarrow Q^{-2}$ | | −170[b] | 340 |
| $Q^- + e^- \rightarrow Q^{-2}$ | | −195[c] | 195 |
| $QH + e^- \rightarrow QH^-$ | | 270[b] | −270 |
| $Q^- + H^+ \rightarrow QH$ | 4.9[d] | | 124 |
| $Q^{-2} + H^+ \rightarrow QH^-$ | 12.7[e] | | −338 |
| $QH^- + H^+ \rightarrow QH_2$ | 10.7[f] | | −218 |
| $Q + e^- + H^+ \rightarrow QH$ | | −269 | 269 |
| $Q + 2e^- + H^+ \rightarrow QH^-$ | | 1 | −1 |
| $Q + 2e^- + 2H^+ \rightarrow QH_2$ | | 220 | −220 |
| $Q^- + e^- + H^+ \rightarrow QH^-$ | | 146 | −146 |
| $QH + e^- + H^+ \rightarrow QH_2$ | | 488 | −488 |
| $Q^- + e^- + 2H^+ \rightarrow QH_2$ | | 360 | −360 |

[a] $\Delta G_{sol}$ is $2.3mk_bT(pH - pK_{a,sol}) - nF(E_h - E_{m,sol})$ (eq 4), and values are given at $E_h = 0$ and pH 7, where $m$ is the number of protons and $n$ is the number of electrons. [b] By analogy with the $E_m$ of trimethyl benozoquinone (*67*). [c] Derived from $E_{m,sol}$ ($Q/Q^-$) and $E_{m,sol}$ ($Q^-/Q^{-2}$). [d] Derived from the p$K_{a,sol}$ for $Q^{-2}/QH^-$ and the $E_{m,sol}$ for $Q^-/Q^{-2}$. [e] Derived from p$K_a$ ($Q^{2-}/QH^-$) being ≈2 units higher than p$K_a$ ($QH^-/QH_2$) (*69*, *72*). Other values are derived as appropriate sums and differences walking around the thermodynamic box (Figure 1). See the Materials and Methods for a more complete derivation of $E_{m,sol}$ and p$K_{a,sol}$ values used here. [f] ref *67*.

protons and electrons transferred, respectively, p$K_a$ and $E_m$ are values for quinone in the protein, and [$R$] and [$P$] are the occupancies of the reactant and product, respectively, calculated by Monte Carlo sampling given the microstate energies in eq 1. To determine the *in situ* $\Delta G$ for each reaction, only conformers for given reactant and product redox states are sampled. For example, to determine $\Delta G$ for the reaction $Q_BH^- + e^- + H^+ \rightarrow Q_BH_2$, only conformers of $Q_BH^-$ and $Q_BH_2$ are allowed. $Q_A$ would be fixed in its oxidized form, and no conformers of $Q_{BD}$ would be allowed in any sampled microstate. There are four conformers with different locations for the protons on $Q_BH^-$ and $Q_BH_2$ (see Figure 5 below). Their accepted occupancies are summed. The reaction free energy is divided into two terms

$$\Delta G = \Delta G_{sol} + \Delta\Delta G_{protein} \quad (3)$$

$\Delta G_{sol}$ is the reference free energy in solution at the given pH and $E_h$. This includes the contributions of the intrinsic quinone proton or electron affinity and the ability of the solvent to donate protons and electrons given the pH and $E_h$. Thus

$$\Delta G_{sol} = 2.3mk_bT(pH - pK_{a,sol}) - nF(E_h - E_{m,sol}) \quad (4)$$

p$K_{a,sol}$ and $E_{m,sol}$ are the quinone reference values in water (Figure 1 and Table 1). $\Delta\Delta G_{protein}$ is the shift in the energy of reduction or protonation as the quinone is moved from water into the protein (*13*, *63*). It is calculated from

$$\Delta\Delta G_{protein} = -2.3k_bT \log\frac{[P]}{[R]} - \Delta G_{sol} \quad (5)$$

$\Delta\Delta G_{protein}$ is due to the changes in quinone p$K_a$ ($\Delta pK_{a,protein}$) and/or $E_m$ ($\Delta E_{m,protein}$). Thus

$$\Delta\Delta G_{protein} = -2.3mk_bT\Delta pK_{a,protein} + nF\Delta E_{m,protein} \quad (6)$$

As the $E_h$ titrations are carried out at pH 7, $\Delta\Delta G_{protein}$ is $nF\Delta E_{m,7}$. The $E_m$ and p$K_a$ values calculated for the quinone in the protein are each viewed as the protein shifting the solution quinone behavior. Thus

$$E_m = E_{m,sol} + \Delta E_{m,protein} \quad (7)$$

$$pK_a = pK_{a,sol} + \Delta pK_{a,protein} \quad (8)$$

For the proton independent half-reactions ($Q + e^- \rightarrow Q^-$, $Q^- + e^- \rightarrow Q^{-2}$, and $QH + e^- \rightarrow QH^-$) $m = 0$ (eq 6); therefore, $\Delta\Delta G_{protein}$ is simply related to the shift in $E_m$ in the protein, $\Delta E_{m,protein} = -\Delta\Delta G_{protein}/nF$ (*63*). When determining $\Delta\Delta G_{protein}$ for the proton-coupled electron transfers (e.g., $Q + e^- + H^+ \rightarrow QH$), $\Delta\Delta G_{protein}$ includes contributions from both $\Delta pK_{a,protein}$ and $\Delta E_{m,protein}$.

Quinone p$K_a$ values can be determined by Monte Carlo sampling as a function of pH (*54*). However, this will not yield the correct free energy of protonation at pH 7 because the protein ionization and conformation are pH-dependent. The free energy of proton-transfer reactions at pH 7 was obtained from the difference between the energy of the electron transfer and the coupled electron- and proton-transfer reaction closing the thermodynamic cycle (Figures 1 and 3) (*73*). For example, the standard free energy of the protonation reaction $Q_B^- + H^+ \rightarrow Q_BH$ at pH 7 is the difference between the $\Delta G$ of $Q_B + e^- + H^+ \rightarrow Q_BH$ and $Q_B + e^- \rightarrow Q_B^-$. A p$K_a'$, the effective p$K_a$ calculated at pH 7, is then obtained from the pH where this $\Delta G$ for the protein would be zero if the protein remained as it is at pH 7

$$pK_a' = 7 - \Delta G/RT \quad (9)$$

The half-reaction $E_m$ and p$K_a$ values were obtained for the relevant quinone reactions in the three binding sites. The energy $\Delta G$ of a particular electron-transfer reaction such as from $Q_A^-Q_B$ to $Q_AQ_B^-$ is then the difference of the redox potentials $E_m$ ($Q_A/Q_A^-$) and $E_m$ ($Q_B/Q_B^-$).

*Factors Contributing to* $\Delta G_{protein}$. In the MCCE analysis, the free-energy change due to the protein (eq 6) can be broken down into

$$\Delta\Delta G_{protein} = (\Delta\Delta G_{rxn} + \Delta G_{pol} + \Delta G_{nonel}) + \Delta G_{res} \quad (10)$$

All terms are changes in the free energy of the reactant and product redox state of the quinone when it is moved from water to the protein. $\Delta\Delta G_{rxn}$, $\Delta G_{pol}$, and $\Delta G_{nonel}$ are independent of the distribution of other conformers and are found in the energy look-up table for each conformer. $\Delta G_{res}$, calculated with eqs 5 and 10, accounts for the changing interaction of the quinone with the protein as it undergoes the redox reaction, as well as the energy needed to keep the conformers and the rest of the protein in equilibrium with the quinone charge and protonation changes. Thus

$$\Delta G_{res} = \Delta G_{res}^{prot} + \Delta G_{prot\rightarrow prot^*}^{red} = \Delta G_{prot\rightarrow prot^*}^{ox} + \Delta G_{res}^{prot^*} \quad (11)$$

If, for example, the reactant is $Q_B$ and the product is $Q_B^-$, $\Delta G_{res}^{prot}$ is the difference in interaction of the protein with $Q_B$ and $Q_B^-$ in the protein equilibrated around $Q_B$ (prot), and $\Delta G_{prot\rightarrow prot^*}^{red}$ is the energy it takes to move the protein into the conformation equilibrated around $Q_B^-$ when the $Q_B$ is reduced (prot*). This is equivalent to reducing $Q_B$ in the prot conformation and then relaxing the protein to the prot*

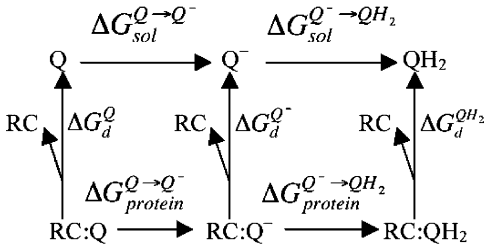


FIGURE 2: Relationship between the equilibrium dissociation energy ($\Delta G_d$) and redox energies of the reaction in solution and in the protein. $\Delta G_d^{Q}$, $\Delta G_d^{Q^-}$, and $\Delta G_d^{QH_2}$ are the dissociation free energies for Q, $Q^-$, and $QH_2$, respectively.

conformation. The reduction could also happen by the alternate path, where first the protein is moved to the conformation equilibrated around $Q_B^-$, while keeping $Q_B$ oxidized requiring $\Delta G^{ox}_{prot\rightarrow prot*}$, and then the quinone is reduced in the pre-prepared protein, prot*, ($\Delta G^{prot*}_{res}$). $\Delta G^{ox}_{prot\rightarrow prot*}$ is always unfavorable, while $\Delta G^{red}_{prot\rightarrow prot*}$ is always favorable. $\Delta G^{prot*}_{red}$ is always more favorable than $\Delta G^{prot}_{res}$ because the cost of rearranging into the protein equilibrated around the product has already been paid (see ref *63* for a more complete discussion).

*Relative Affinity of Different Quinone Redox States.* Each quinone redox state has a different affinity for each binding site required for RC function. To the degree that the protein stabilizes the reactant or product state in an electron- or proton-transfer process, it will bind that species more tightly (Figure 2) (*74*). For example, $\Delta\Delta G_{protein}$ for the $Q + e^- \rightarrow Q^-$ reaction provides a measurement of the relative affinities of Q and $Q^-$ for the binding site

$$\Delta\Delta G_{protein} = \Delta G_d^{Q} - \Delta G_d^{Q^-} = \Delta G_{protein}^{Q\rightarrow Q^-} - \Delta G_{sol}^{Q\rightarrow Q^-} = 2.303RT(\log K_d^{Q^-} - \log K_d^{Q}) \quad (12)$$

$\Delta G_d$ is the dissociation energy for each species, and $K_d$ is the derived dissociation constant for Q and $Q^-$.

## RESULTS

*Energy of Ubiquinone Reduction at $Q_B$ Proximal, $Q_B$ Distal, and $Q_A$ Sites: First Reduction of $Q_B$ in the Proximal Binding Site.* The inner, proximal $Q_B$ site is calculated to stabilize quinone reduction to the anionic semiquinone by −138 meV relative to the same reaction in water ($\Delta\Delta G_{protein}$) (values are given to the nearest millielectronvolt only as an aid for tracking the connections between the numbers). Using a solution reference $E_m$ ($E_{m,sol}$) of −145 mV (Table 1), the $E_m$ in the protein would be −7 mV (eq 7, Tables 2a and 5a) in good agreement with the experimentally determined value of ≈30 mV (*75*). $\Delta\Delta G_{protein}$ can be divided into the loss of stabilization of the charge by water when the cofactor moves from the solution ($\Delta\Delta G_{rxn}$), the electrostatic pairwise interactions with the protein backbone ($\Delta G_{pol}$) and residues and ligands ($\Delta G_{res}$), and the torsion and Lennard−Jones interactions ($\Delta G_{nonel}$) (eq 10). $\Delta G_{res}$ includes the direct interactions between residues and the quinone as well as the energy required to change the residue conformation and ionization states so they remain in equilibrium in each quinone redox state (eq 11, Table 3).

For the first $Q_B$ reduction, $\Delta\Delta G_{rxn}$ is ≈390 meV and $\Delta G_{pol}$ is ≈−390 meV, with the backbone dipoles essentially compensating for the removal from water (*43*, *76*, *77*) (Table 3). The primary contribution to $\Delta G_{pol}$ is from residues L210−247 (helix E), with smaller contributions from the stretches M136−162 and M232−288. Pairwise interactions with other side chains and ligands ultimately favor reduction by −140 meV (Table 2a). The +2 charge of the nearby non-heme iron provides a constant term favoring ionization of the proximal $Q_B$. However, other residues must undergo changes in ionization and conformation for $Q_B^-$ to be stabilized.

Monte Carlo sampling in MCCE maintains the ionization states and position of surrounding residues in equilibrium with the quinone redox states. If the protein was fixed in the conformation and ionization equilibrated in the ground $Q_B$ state, $\Delta G^{prot}_{res}$ is 86 meV (Table 3). Combining this with $\Delta\Delta G_{rxn}$, $\Delta G_{pol}$, and $\Delta G_{nonel}$, which are independent of the chosen conformers of other residues, yields $\Delta\Delta G_{protein}$ of 83 meV (eq 10). Adding the $E_{m,sol}$ of −145 mV yields an $E_m$ for $Q_B$ in the ground-state protein of −228 mV, indicating a very destabilized $Q_B^-$ (eq 10, Table 3). This is consistent with earlier calculations (*37*) as well as the observation that in dark-adapted, frozen RCs $Q_B$ cannot be reduced by $Q_A$ (*78*, *79*). It takes 183 meV to move the protein from the conformation equilibrated around $Q_B$ to one equilibrated around $Q_B^-$ without reducing the quinone ($\Delta G^{ox}_{prot\rightarrow prot*}$) (Table 3). Reduction in the pre-prepared protein would be stabilized by $\Delta G^{prot*}_{res}$ and would be very favorable, with a resultant $E_m$ of 318 mV. The calculated reaction $\Delta G_{res}$, −135 meV, is much less favorable (eq 11, Table 2a) because it includes the work to rearrange the protein from the reactant to product conformation.

Proton uptake to surrounding residues, in particular, GluL212 and AspL213, is the most important change required to stabilize $Q_B^-$. As found in earlier calculations (*37*), a net charge of −1 is maintained on these two acids and $Q_B$. In these simulations, when $Q_B$ is oxidized, GluL212 is ionized and AspL213 is protonated (Appendix I in the Supporting Information). When $Q_B$ is ionized, both acids are neutral. The orientation of the hydroxyl SerL223, which can offer a hydrogen bond to either AspL213 or $Q_B$ also changes on reduction (Table 4). SerL223 hydroxyl positions that can donate a hydrogen bond to and accept a hydrogen bond from the neutral $Q_B$ are accepted by Monte Carlo sampling (Table 4). When $Q_B$ is reduced, SerL223 becomes a hydrogen-bond donor to the anionic semiquinone.

*Protonation of the Anionic Semiquinone.* QH and Q interact with the $Q_B$ site similarly (Table 2a). The ionization of the acidic cluster of GluL212 and AspL213 are the same with $Q_BH$ or $Q_B$ (Appendix I in the Supporting Information). The small differences in $\Delta\Delta G_{rxn}$ are due to differences in the charge distribution in the two quinone species (*44*). The differences in Lennard−Jones interactions ($\Delta G_{nonel}$) and $\Delta G_{res}$ come from the interactions of the quinone proton with the protein. Three positions are acceptable with the majority of the quinones in Monte Carlo sampling donating a hydrogen bond to SerL223 (Table 4). The proximal $Q_B$ site is designed to stabilize anions, stabilizing $Q_B^-$ better than $Q_B$ or QH. The free energy of protonating $Q_B^-$ is 255 meV at pH 7 (Figure 3). This shifts the quinone $pK_a'$ from 4.9 in solution to 2.7 in the protein (eq 9); therefore, the quinone will remain deprotonated as is found.

Table 2: MCCE-Calculated Redox Energies of Quinone in Proximal and Distal $Q_B$ and $Q_A$ Sites at pH 7 and $E_h = 0$ with P, the Bacteriochlorophyll Dimer, Neutral[a]

(a) $Q_B$ Proximal Site

| half-reaction | $\Delta\Delta G_{rxn}$ | $\Delta G_{pol}$ | $\Delta G_{nonel}$ | $\Delta G_{res}$ | $\Delta\Delta G_{protein}$ | $\Delta G_{sol}$ | $\Delta G_{calc}$ | $\Delta\log K_d$ |
|---|---|---|---|---|---|---|---|---|
| $Q_B \rightarrow Q_B^-$ | 386 | −389 | 0 | −135 | −138 | 145 | 7 | −2.4 |
| $Q_B + e^- + H^+ \rightarrow Q_BH$ | −15 | 74 | −23 | −43 | −7 | 269 | 262 | −0.1 |
| $Q_B + 2e^- \rightarrow Q_B^{-2}$ | 1471 | −783 | 0 | −533 | 155 | 340 | 495 | 2.6 |
| $Q_B + 2e^- + H^+ \rightarrow Q_BH^-$ | 429 | −342 | −18 | −179 | −110 | −1 | −111 | −1.8 |
| $Q_B + 2e^- + 2H^+ \rightarrow Q_BH_2$ | 18 | 117 | −48 | −38 | 49 | −220 | −171 | 0.8 |
| $Q_{B-} + e^- \rightarrow Q_B^{-2}$ | 1085 | −394 | 0 | −398 | 293 | 195 | 488 | 5 |

(b) $Q_B$ Distal Site

| half-reaction | $\Delta\Delta G_{rxn}$ | $\Delta G_{pol}$ | $\Delta G_{nonel}$ | $\Delta G_{res}$ | $\Delta\Delta G_{protein}$ | $\Delta G_{sol}$ | $\Delta G_{calc}$ | $\Delta\log K_d$ |
|---|---|---|---|---|---|---|---|---|
| $Q_{BD} \rightarrow Q_{BD}^-$ | 317 | −219 | 0 | 19 | 117 | 145 | 262 | 2.0 |
| $Q_{BD} + e^- + H^+ \rightarrow Q_{BD}H$ | −20 | −16 | −8 | −15 | −59 | 269 | 210 | −1.0 |
| $Q_{BD} + 2e^- \rightarrow Q_{BD}^{-2}$ | 1130 | −433 | 0 | −121 | 576 | 340 | 916 | 9.7 |
| $Q_{BD} + 2e^- + H^+ \rightarrow Q_{BD}H^-$ | 365 | −233 | −8 | −63 | 61 | −1 | 60 | 1.0 |
| $Q_{BD} + 2e^- + 2H^+ \rightarrow Q_{BD}H_2$ | 15 | −35 | −18 | 8 | −30 | −220 | −250 | −0.5 |

(c) $Q_A$ Site

| half-reaction | $\Delta\Delta G_{rxn}$ | $\Delta G_{pol}$ | $\Delta G_{nonel}$ | $\Delta G_{res}$ | $\Delta\Delta G_{protein}$ | $\Delta G_{sol}$ | $\Delta G_{calc}$ | $\Delta\log K_d$ |
|---|---|---|---|---|---|---|---|---|
| $Q_A \rightarrow Q_A^-$ | 390 | −254 | 0 | −244 | −108 | 145 | 37 | −1.8 |
| $Q_A + e^- + H^+ \rightarrow Q_AH$ | −13 | 19 | −15 | −10 | −19 | 269 | 250 | −0.3 |
| $Q_A + 2e^- \rightarrow Q_A^{-2}$ | 1479 | −494 | 0 | −588 | 397 | 340 | 737 | 6.7 |
| $Q_A + 2e^- + H^+ \rightarrow Q_AH^-$ | 430 | −219 | −16 | −8 | −13 | −1 | −14 | −0.2 |
| $Q_A + 2e^- + 2H^+ \rightarrow Q_AH_2$ | 18 | 13 | −21 | −12 | −2 | −220 | −222 | −0.03 |

[a] $\Delta G_{sol}$ ($E_h = 0$, pH 7) is calculated as $2.3mk_bT(7 - pK_{a,sol}) - nF(0 - E_{m,sol})$ (eq 4) using $pK_{a,sol}$ and $E_{m,sol}$ from Table 1. For protonated quinones, $\Delta\Delta G_{rxn}$ and $\Delta G_{pol}$ are the values for the four conformers with different proton positions weighted by their occupancies in Monte Carlo sampling (Figure 5 and Table 4). $\Delta\Delta G_{protein}$ was calculated with eq 5, and $\Delta G_{res}$ was calculated with eq 10. (a) $pK_a'$ ($pK_a$ calculated from the energy of protonation at pH 7 (eq 9) for $Q_B^-$, 2.7; for $Q_B^{-2}$, 17.3; and for $Q_BH^-$, 8.0. (b) $pK_a'$ for $Q_{BD}^-$, 7.9; for $Q_{BD}^{-2}$, 21.4; and for $Q_{BD}H^-$, 12.2. (c) $pK_a'$ for $Q_A^-$, 3.4; for $Q_A^{-2}$, 19.7; and for $Q_AH^-$, 8.8.

Table 3: Energy of Protein Rearrangement on Quinone Reduction to Semiquinone in Three Binding Sites[a]

| half-reaction | $\Delta G_{res}$ | $\Delta G_{res}^{prot}$ | $\Delta G_{res}^{prot*}$ | $\Delta G_{prot\rightarrow prot*}^{red}$ | $\Delta G_{prot\rightarrow prot*}^{ox}$ |
|---|---|---|---|---|---|
| $Q_AQ_B + e^- \rightarrow Q_AQ_B^-$ | −135 | 86 | −318 | −221 | 183 |
| $Q_AQ_{BD} + e^- \rightarrow Q_AQ_{BD}^-$ | 19 | 69 | −74 | −50 | 93 |
| $Q_AQ_B + e^- \rightarrow Q_A^-Q_B$ | −244 | −263 | −279 | −19 | 35 |

[a] $\Delta G_{res}$ was calculated with eq 10. Other terms were calculated with eq 11. $\Delta G_{res}^{prot}$ is the difference in interaction of the protein with quinone and semiquinone in the protein equilibrated around the quinone (prot), and $\Delta G_{prot\rightarrow prot*}^{red}$ is the energy it takes to move the protein into the conformation equilibrated around the semiquinone (prot*). The reduction could also happen by the alternate path, where first the protein is moved to the conformation equilibrated around the semiquinone requiring $\Delta G_{prot\rightarrow prot*}^{ox}$ and then the quinone is reduced in the pre-prepared protein, prot*, ($\Delta G_{res}^{prot*}$) (*63*).

Table 4: Position of Hydroxyl Proton on SerL223 and Proximal $Q_B$ Found in Monte Carlo Sampling for the Different $Q_B$ Redox States[a]

| | $Q_B$ | | | | SerL223 | |
|---|---|---|---|---|---|---|
| redox state | H1 | H2 | H3 | H4 | A | B |
| $Q_B$ | | | | | 0.20 | 0.80 |
| $Q_B^-$ | | | | | 0.00 | 1.00 |
| $Q_B^{-2}$ | | | | | 0.00 | 1.00 |
| $Q_BH$ | 0.54 | 0.16 | 0.00 | 0.30 | 0.56 | 0.44 |
| $Q_BH^-$ | 0.08 | 0.72 | 0.00 | 0.20 | 0.07 | 0.93 |
| $Q_BH_2$ | 0.60 | 0.40 | 0.00 | 1.00 | 0.68 | 0.32 |

[a] See Figure 5 for hydrogen locations. Monte Carlo sampling carried out at pH 7 with the quinone redox state fixed.

*Second Reduction of $Q_B$.* The two-electron quinone reduction is calculated to be 155 meV less favorable in the $Q_B$ site than in solution (Table 2a). $Q_B^{-2}$ is destabilized 1471 meV by $\Delta\Delta G_{rxn}$, ≈4 times that found for $Q_B^-$, while the favorable $\Delta G_{pol}$ is −783 meV, only twice that of the semiquinone. This is as expected given the linear response of the CE calculations used for the interaction of the static portions of the protein with the quinone charge. Thus, the pairwise interactions for groups with no conformation or ionization changes double as the charge on the quinone doubles. At the same time, the Born reaction field energy increases as $\approx q^2$; therefore, it costs 4 times more energy to bury a charge of −2 than −1 (*80*). However, MCCE interactions with parts of the protein such as GluL212 and SerL223 that change do not show a linear response to changes in the charge. $\Delta G_{res}$ for $Q_B + e^- \rightarrow Q_B^-$ is much less favorable than $\Delta G_{res}^{prot*}$, because work is done to modify the $Q_B$ site residues (eqs 10 and 11). However, there are only small changes in the position and ionization states of residues in the $Q_B$ site on the second reduction. Only GluH173 becomes partially protonated to stabilize the dianion (Appendix I in the Supporting Information); therefore, little additional work is done to stabilize $Q_B^{-2}$. Thus, $\Delta G_{res}^{prot} \approx \Delta G_{res}^{prot*}$ for $Q_B^- + e^- \rightarrow Q_B^{-2}$ and $\Delta G_{res}^{prot}$ for $Q_B^- + e^- \rightarrow Q_B^{-2}$ is approximately twice $\Delta G_{res}^{prot*}$ for $Q_B + e^- \rightarrow Q_B^-$. This illustrates how the resultant interaction of the quinone with the site, $\Delta G_{res}$, is largest when the site is pre-prepared ($\Delta G_{prot\rightarrow prot*}^{red} \approx 0$). However, even the added stabilization of the dianion because of the reaction occurring in a prepared protein is insufficient to pay for the much larger reaction field penalty. If the $E_{m,sol}$ is −195 mV, then the $E_m$ for the second reduction of the anionic quinone ($Q^- + e^- \rightarrow Q^{2-}$) is −488 mV.

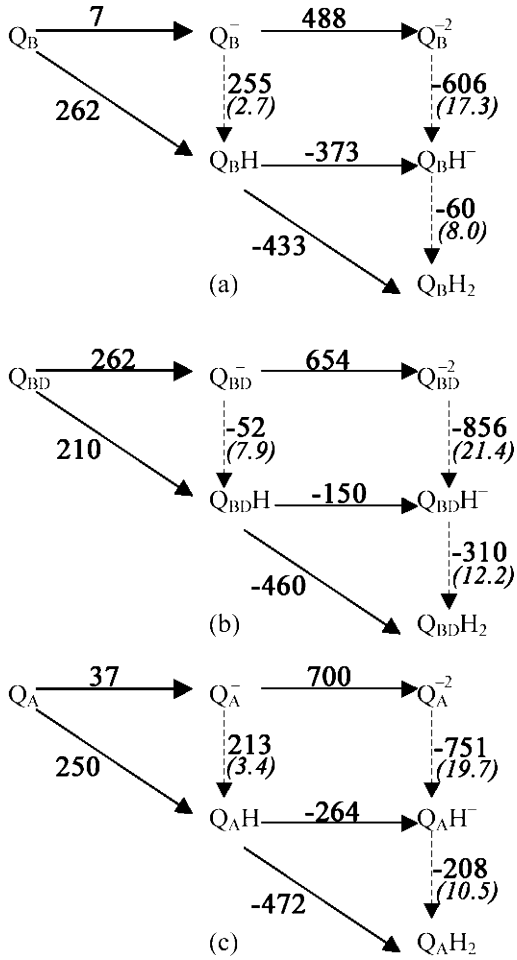


FIGURE 3: MCCE-calculated quinone redox energies in the three binding sites. (a) $Q_B$ proximal site. (b) $Q_{BD}$ distal site. (c) $Q_A$ site. Horizontal arrows, electron transfers; dashed vertical arrows, proton transfers; diagonal arrows, proton-coupled electron transfers. $\Delta G$ values between all states connected by solid arrows were calculated by Monte Carlo sampling of the reactant and product states as a function of $E_h$. $\Delta G$ values of protonation reactions were obtained by closing the appropriated thermodynamic cycles. $pK_a'$ values (in parentheses) were obtained from the $\Delta G$ of protonation at pH 7 using eq 9.

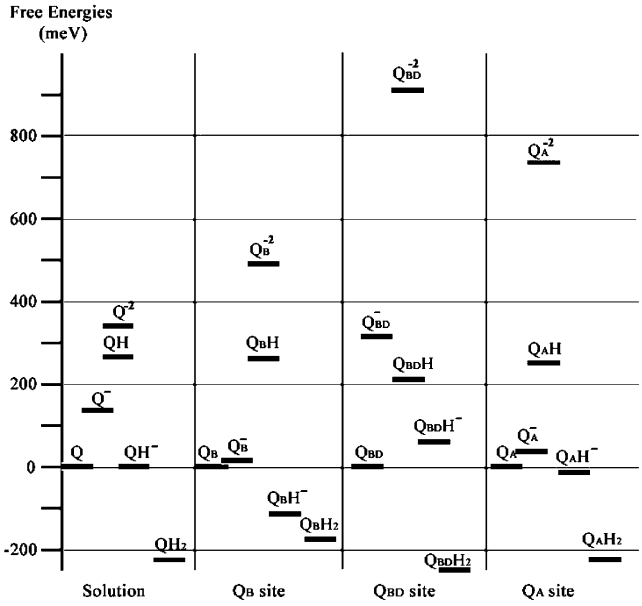


FIGURE 4: Energy levels of quinone products in $Q_B$, $Q_{BD}$, and $Q_A$ sites. Values are from Table 2.

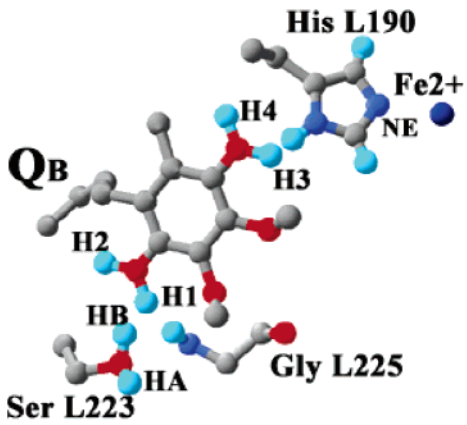


FIGURE 5: Available hydroxyl positions in different conformers of SerL223 and in QH and $QH_2$ states of ubiquinone. The UQ protons: H1, H2, H3, and H4. SerL223 protons: HA and HB. The side chain of the ligand HisL190 and the backbone of GlyL225 are also shown. The protein coordinates are taken from the 1AIJ structure (*21*) with the quinone moved into the 1AIG proximal position as described in the Materials and Methods.

*Protonation State of the Double-Reduced $Q_B$.* The single-protonated fully reduced quinone, $Q_BH^-$, is stabilized by −111 meV, interacting with the protein in a manner similar to that found for the semiquinone (Table 2a). The ionization states in the acidic cluster are the same as with $Q_B^-$ (Appendix I in the Supporting Information). The $pK_a$ for binding the first proton to $Q^{-2}$ is 12.7 in solution. The $pK_a'$ is calculated to be pushed up to 17.3 in the $Q_B$ site because of the destabilization of $Q_B^{-2}$ (Table 2a and Figure 3).

The fully protonated, fully reduced $Q_BH_2$ is destabilized 49 meV by the protein. The interaction with the backbone ($\Delta G_{pol}$) in particular with GlyL225 accounts for much of this unfavorable interaction. The $pK_a$ of $QH^-$ in solution is 10.7, but $pK_a'$ is only 8.0 in the protein, a reflection of the destabilization of the second bound proton.

*Location of Protons on $Q_B$.* The quinone makes 2 hydrogen bonds in the $Q_B$ site. One is to HisL190, which lies between the non-heme ferrous iron and $Q_B$. The other quinone carbonyl interacts with SerL223 and the backbone nitrogen of GlyL225. There are 4 positions for hydrogen sampled on $Q_B$ (Figure 5). It can donate a hydrogen bond to (H1) or accept a hydrogen bond from (H2) SerL223, or on the carbonyl proximal to the non-heme iron, it can point toward (H3) or away from (H4) HisL190. Two of the seven possible SerL223 conformers are occupied. In one, it is a donor to AspL213 and can be a hydrogen-bond acceptor from a protonated quinone (A), and in the other, it donates a hydrogen bond to $Q_B$ (B). When $Q_B$ is protonated, the position of protons on the Ser and the nearby quinone carbonyl are correlated to avoid clashes.

In the $Q_B$ ground state, SerL223 donates a proton to $Q_B$ (position B) with 80% probability (Table 4). This preference is strengthened in any of the anionic $Q_B$ states. The SerL223 hydroxyl in the A position destabilizes $Q_B^-$ by 67 meV, while the hydroxyl in the B position stabilizes it by −114 meV. A better test of the importance of the SerL223 position can be gained by comparing the $E_m$ calculated with the Ser proton fixed, allowing the rest of the protein to come to equilibrium around each hydroxyl position. The $E_m$ with SerL223 B is

−5 mV, essentially unchanged from that found in the free calculation. If the SerL223 is fixed in the A conformation, then the $E_m$ is lowered to −95 mV. Thus, as proposed previously (*81*), if the SerL223 is oriented to donate a hydrogen bond to AspL213 and not to $Q_B$ in the ground state, $Q_B$ reduction by $Q_A$ would be unfavorable.

In the neutral species $Q_BH$ and $Q_BH_2$, there is a distribution of quinone hydroxyl positions found in Monte Carlo sampling. It is somewhat more likely that the quinone will be a proton donor to SerL223. However, different positions are found because there are several competing energy terms. No individual hydrogen bond between neutral $Q_B$ and SerL223 is stronger than 2 kcal/mol; therefore, multiple orientations have similar energies. The only disallowed quinone proton position is the one that clashes with the hydrogen from HisL190 (H3). Thus, $Q_BH$ H2, where the quinone accepts a hydrogen bond from SerL223, has a better interaction with the backbone amide of GlyL225 and with SerL223 than H1, where the quinone donates a hydrogen bond to SerL223. However, H1 is found more often in Monte Carlo sampling because the correlated SerL223 position, A, has a more favorable interaction with AspL213. In addition, there is room for a proton in the region near HisL190 on the other carbonyl (H4), and this position is sufficiently favorable that it is partially occupied in $Q_BH$ and $Q_BH^-$. Favorable Lennard−Jones interactions with HisL190 ($\Delta G_{nonel}$) stabilize this position.

*Relative Affinity of the Different Redox States of Quinone for the $Q_B$ Site.* The difference in interaction of the quinone and another, product redox state with the protein is provided by $\Delta\Delta G_{protein}$ for that reaction (Table 2). Thus, the binding energies of the two species differ by $\Delta\Delta G_{protein}$ (eq 12, Figure 2). For example, when $Q_B$ and $Q_B^-$ are compared, $\Delta\Delta G_{protein}$ is −138 meV, indicating that the semiquinone interacts 3.2 kcal/mol more favorably and will thus bind 220 times more tightly to the binding site (eq 12). This is in agreement with experimental data, showing that $Q_B^-$ is more tightly bound then $Q_B$ or $Q_BH_2$ (*19*). $\Delta\Delta G_{protein}$ is similar for $Q_B^-$ or $Q_BH^-$ and so their relative affinities for the binding site will be similar. Again, because $\Delta\Delta G_{protein}$ is similar for $Q_B$ and $Q_BH$, there will be little difference in these $K_d$ values (*82*). For $Q_BH_2$, the $\Delta\Delta G_{protein}$ of 49 meV shows that the dihydroquinone is more stable in solution, keeping $Q_BH_2$ 7 times less tightly bound than $Q_B$.

*Redox Reactions in the Distal $Q_B$ Site.* There are different $Q_B$-binding sites found in X-ray crystal structures (*12*, *21*). In wild-type RCs, two distinct $Q_B$-binding sites (distal and proximal to the non-heme iron) have been described. In the charge-separated $P^+Q_AQ_B^-$ structure (1AIG), the inner proximal semiquinone $Q_B^-$ is located ≈5 Å closer to $Q_A$ than it is in the dark-adapted $PQ_AQ_B$ outer, distal site (1AIJ) and it has undergone a 180° propeller twist around the isoprene chain. In this outer site, the quinone is making hydrogen bonds with IleL224 and AlaL186.

The energetics of quinone reduction and protonation at the distal site ($Q_{BD}$) were calculated using the original distal, quinone position in 1AIJ. The $E_m$ for the $Q_{BD} + e^- \rightarrow Q_{BD}^-$ half-reaction is −262 mV, while it is −7 mV in the proximal site (Table 2). The $Q_B$ site stabilizes the semiquinone anion by −138 meV, while the $Q_{BD}$ site destabilizes it by 117 meV (Table 2). When the two sites are compared, there is 80 meV less reaction field loss in $Q_{BD}$ but 180 meV less favorable $\Delta G_{pol}$ and 255 meV more unfavorable interactions with the rest of the protein. Reduction with residues in the protein equilibrated around the oxidized quinone, $\Delta G$, is less unfavorable in the distal than the proximal site because the quinone is further from the acidic cluster of GluL212 and AspL213 (Table 3). However, the relaxation around the reduced quinone, $\Delta G^{ox}_{prot\rightarrow prot^*}$, provides far less stabilization. As in the proximal site, motions of SerL223 and protonation of GluL212 stabilize $Q_{BD}^-$. However, with an anionic semiquinone in the $Q_{BD}$ site, GluL212 remains 70% ionized, destabilizing the anionic quinone by ≈90 meV (Table 2b, Appendix I in the Supporting Information).

The energies of the other redox states of $Q_{BD}$ show that the distal site destabilizes anionic quinones, while the neutral protonated $Q_{BD}H$ and $Q_{BD}H_2$ are stabilized more than in the proximal $Q_B$ site (Figures 3 and 4). There is adequate room in the binding site to protonate either carbonyl, although the position pointing toward the IleL224 HN is disallowed. $Q_{BD}^{-2}$ is 421 meV higher in energy than $Q_B^{-2}$. The desolvation penalty for the fully reduced quinone is smaller in the distal site, but the stabilizing interactions with the backbone and other residues are much smaller. The dihydroquinone is however stabilized relative to the solution by −30 meV in the distal site, while it is destabilized by 49 meV in proximal site. Thus, $QH_2$ will be bound 3 times more tightly in the distal site than is the quinone (Table 2 and Figure 3).

*$Q_A$ Redox Reactions.* In bacterial RCs, $Q_A$ is tightly bound to the protein, and the $Q_A$ position is well-defined in all crystal structures. The quinone is making hydrogen bonds to HisL219 and the backbone of AlaM260. The protein stabilizes reduction of $Q_A$ by −108 meV relative to the quinone in solution (Table 2c). Given $E_{m,sol}$ for $Q/Q^-$ of −145 mV, this results in an $E_m$ of −37 mV close to the measured values of −45 (*83*) to −75 mV (*75*) at pH 7. $\Delta\Delta G_{rxn}$ destabilizes the anionic semiquinone by 390 meV, the same as found in the proximal $Q_B$ site. Interactions with backbone dipoles stabilize reduction by −254 meV. The primary contributions are from amides M260−271, in the loop leading into and the first 10 residues of the E transmembrane helix. $\Delta G_{res}$ is −244 meV. Reduction of $Q_A$ is favored even in the protein equilibrated with the oxidized quinone ($\Delta G^{prot}_{res}$) (Table 3), in agreement with the ability of the dark adapted, frozen protein to form $Q_A^-$ following activation of the RCs with light (*84*). $\Delta G^{ox}_{prot\rightarrow prot^*}$ is 35 meV, showing there are only small rearrangements in the MCCE calculation on $Q_A$ reduction. Several polar residues including ThrM261, ThrM222 and TyrH40 rearrange their hydroxyl dipoles to stabilize the charge. The resultant $\Delta\Delta G_{protein}$ of −108 meV indicates that $Q_A^-$ will be bound 72 times tighter than $Q_A$.

There are a variety of studies that suggest a linkage between $Q_A$ and $Q_B$ (*1*, *85*). The $E_m$ for $Q_A$ is slightly less negative when $Q_B$ is reduced than when it is oxidized (Table 5a). The charge−charge interaction between $Q_A^-$ and $Q_B^-$ itself lowers the $E_m$ by ≈55 mV. However, neutralization of GluL212 in the $Q_B$-site acidic cluster raises the potential by ≈62 mV. The resultant $E_m$ thus changed by only ≈10 mV when $Q_B$ is reduced.

As in the proximal $Q_B$ site, the $Q_A$ site stabilizes species with a −1 charge relative to the neutral or doubly reduced

Table 5: Selected Quinone Half-Reactions Calculated at pH 7

| half-reactions[a] | $E_{m,sol}$ (mV) | $\Delta G_{sol}$ (meV) | $\Delta G_{protein}$ (meV) | $E_m$ (mV) | $\Delta G$ (meV) |
|---|---|---|---|---|---|
| $\mathbf{Q_A}Q_B + e^- \rightarrow \mathbf{Q_A}^-Q_B$ | −145 | 145 | −108 | −37 | 37 |
| $\mathbf{Q_A}Q_B^- + e^- \rightarrow \mathbf{Q_A}^-Q_B^-$ | −145 | 145 | −121 | −24 | 24 |
| $\mathbf{Q_A}Q_BH + e^- \rightarrow \mathbf{Q_A}^-Q_BH$ | −145 | 145 | −113 | −32 | 32 |
| $Q_A\mathbf{Q_B} + e^- \rightarrow Q_A\mathbf{Q_B}^-$ | −145 | 145 | −137 | −7 | 7 |
| $Q_A^-\mathbf{Q_B} + e^- \rightarrow Q_A^-\mathbf{Q_B}^-$ | −145 | 145 | −144 | −1 | 1 |
| $Q_A\mathbf{Q_B}^- + e^- \rightarrow Q_A\mathbf{Q_B}^{-2}$ | −195 | 195 | 295 | −490 | 490 |
| $Q_A\mathbf{Q_BH} + e^- \rightarrow Q_A\mathbf{Q_BH}^-$ | 270 | −270 | −103 | 373 | 373 |
| $Q_A\mathbf{Q_B} + e^- + H^+ \rightarrow Q_A\mathbf{Q_BH}$ | | 269 | −7 | | 262 |
| $Q_A^-\mathbf{Q_B} + e^- + H^+ \rightarrow Q_A^-\mathbf{Q_BH}$ | | 269 | −10 | | 259 |
| $Q_A\mathbf{Q_B}^- + e^- + H^+ \rightarrow Q_A\mathbf{Q_BH}^-$ | | −146 | 24 | | −122 |
| $Q_A\mathbf{Q_BH} + e^- + H^+ \rightarrow Q_A\mathbf{Q_BH_2}$ | | −488 | 56 | | −433 |

| reactions[b] | derived from | $\Delta G$ (meV) | exp. $\Delta G$ (meV) |
|---|---|---|---|
| $Q_AQ_B + e^- \rightarrow Q_A^-Q_B$ | $\Delta G_1$[a] | 37 | 45 (*83*) to 75 (*75*) |
| $Q_A^-Q_B \rightarrow Q_AQ_B^-$ | $\Delta G_4 - \Delta G_1$ | −30 | −70 (*86*−*88*) |
| $Q_AQ_B^- + e^- \rightarrow Q_A^-Q_B^-$ | $\Delta G_2$[c] | 24 | 20 (*75*) |
| $Q_A^-Q_B^- \rightarrow Q_AQ_B^{-2}$ | $\Delta G_6 - \Delta G_2$ | 464 | >240[d] |
| $Q_A^-Q_B^- + H^+ \rightarrow Q_A^-Q_BH$ | $\Delta G_9 - \Delta G_5$ | 258 | 150 (*90*)[e] |
| $Q_AQ_B^{-2} + H^+ \rightarrow Q_AQ_BH^-$ | $\Delta G_{10} - \Delta G_6$ | −620 | >−215[d] |
| $Q_A^-Q_BH \rightarrow Q_AQ_BH^-$ | $\Delta G_7 - \Delta G_3$ | −405 | −250 ± 40 (*90*) |
| $Q_AQ_BH^- + H^+ \rightarrow Q_AQ_BH_2$ | $\Delta G_{11} - \Delta G_7$ | −60 | −90 ± 18 (*89*, *92*)[f] |

[a] MCCE-calculated redox midpoint potential of selected half-reactions involving reduction of the proximal $Q_B$. The quinone that is undergoing the redox reaction is in bold. An unchanged, charged quinone is italicized. [b] Calculated free energy of the electron- and proton-transfer reactions in bacterial RC. $\Delta G$ values derived from appropriate half-reactions (Table 5a and Figure 6). [c] $\Delta G$ calculated for the reaction at $E_h = 0$; therefore, $\Delta G = -nFE_m$. [d] Personal communication with C. A. Wraight. [e] $\Delta G$ at pH 7 derived from the estimated $\Delta G$ of 180 ± 30 meV at pH 7.5 (*90*).[f] $\Delta G$ at pH 7 derived from the measured p$K_a$ of 8.5 ± 0.3 (*89*, *92*).

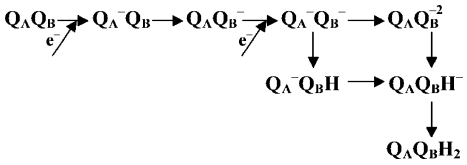


FIGURE 6: Electron- and proton-transfer reactions in bacterial RCs. The free energy of the proton transfer $Q_A^-Q_B^- + H^+ \rightarrow Q_A^-Q_BH$ is calculated from the free-energy difference between the reactions $Q_A^-Q_B^- + H^+ \rightarrow Q_AQ_BH^-$ and $Q_A^-Q_BH \rightarrow Q_AQ_BH^-$.

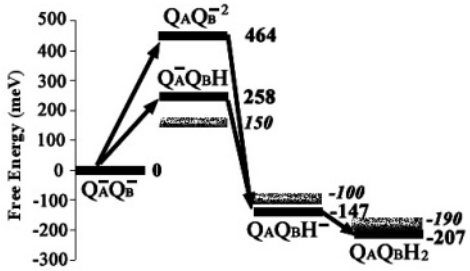


FIGURE 7: Comparison of calculated and experimental energy levels for doubly reduced states. Solid lines, the MCCE-calculated free energies (Table 5b); and gray lines, experimental energy values (see Table 5b for details).

forms of the quinone. Protonation of $Q_A$ is more favorable then $Q_B$ with a p$K_a'$ of 3.4. There is adequate room in the binding site to protonate either carbonyl, although protonation of the carbonyl near AlaM260 is favored. The site destabilizes the dianion by 397 meV (Table 2c), significantly more than the $Q_B$ site.

*Energetics of the Electron Transfers between $Q_A$ and $Q_B$: First Electron Transfer, $Q_A^-Q_B \rightarrow Q_AQ_B^-$.* In RCs, $Q_A$ is reduced forming $Q_A^-Q_B$, and then the electron is transferred to $Q_B$ yielding $Q_AQ_B^-$ (Figure 6). The MCCE calculated $E_m$ values for $Q_AQ_B/Q_A^-Q_B$ and $Q_AQ_B/Q_AQ_B^-$ half-reactions are −37 and −7 mV (Table 5a). The free-energy difference, $\Delta G$, for $Q_A^-Q_B \rightarrow Q_AQ_B^-$ is −30 meV (Table 5b), close to the experimental results of ≈−70 meV determined from the rate of $P^+Q_B^-$ charge recombination, which proceeds via an equilibrated, thermal reduction of $Q_A$ (*86*−*88*). Any uncertainties in $E_{m,sol}$ for $Q/Q^-$ cancel in the calculated $\Delta G$. $Q_A$ and $Q_B$ are arranged with $c_2$ symmetry around the non-heme iron. The two sites have similar $\Delta\Delta G_{rxn}$. However, $Q_B^-$ has a much more favorable interaction with the backbone amide dipoles, $\Delta G_{pol}$, while $Q_A^-$ has a more favorable interaction with the residues of the protein (Table 2). The result is that, following the rearrangements of the $Q_B$ site, the first electron transfer from $Q_A^-$ to $Q_B$ is favorable.

*Second Electron Transfer and Subsequent Protonation, $Q_A^-Q_B^- \rightarrow Q_AQ_BH_2$.* The second electron transfer results in the state $Q_AQ_BH^-$ (Figure 6) (*29*, *89*). A mechanism where $Q_B^-$ is protonated forming $Q_BH$, followed by the second electron transfer, is supported by the free energy and pH dependence of the rate of the reduction of $Q_B^-$ by $Q_A^-$ (*16*). This conclusion is also supported by the analysis of the pH dependence of rhodoquinone (RQ) reduction in the $Q_B$ site. The p$K_a$ of RQ in solution is 7.3 ± 0.2, binding a proton more tightly then UQ (*90*). The pH dependence of the rate of the second electron transfer shows that $RQ_BH$ is an intermediate when RQ is substituted for UQ. The free energy calculated here for $Q_A^-Q_B^- \rightarrow Q_AQ_B^{-2}$ of 464 meV versus $Q_A^-Q_B^- \rightarrow Q_A^-Q_BH$ of 258 meV supports the mechanism with proton transfer before electron transfer at pH 7 (Figure 7). These results are also consistent with prior electrostatic calculations in *Rps. viridis* RCs (*91*).

The free-energy change for $Q_A^-Q_B^- \rightarrow Q_A^-Q_BH$ was estimated to be 180 meV at pH 7.5 from a Marcus analysis comparing the electron-transfer rates when RQ and UQ are in the $Q_B$ site (*90*). This would give a $\Delta G$ of 150 meV at pH 7 and a p$K_a'$ for $Q_B^-$ of 4.5. It is calculated to require 258 meV to protonate $Q_B^-$, 110 meV more than the value derived from the experiment. The calculated p$K_a'$ for $Q_B^- \rightarrow Q_BH$ is 2.7. The unfavorable energy for the protonated

semiquinone could arise from the proton position not being properly optimized in the calculations or from the negative charge on the semiquinone being overly stabilized. However, a high energy for $Q_BH$ is not ruled out by the observed rate for the second reduction of $Q_B$. The rate is proportional to the product of the concentration of $Q_A^-Q_BH$ and the rate of electron transfer from $Q_A^-$ to $Q_BH$ (*12*). If the $Q_A^-Q_BH$ level is 110 meV higher as suggested here, its concentration will be 70 times smaller. To maintain the same $Q_A^-Q_B^- \rightarrow Q_A^-Q_BH$ reaction rate [$k_{AB}^{(2)} \approx 10^3$ s$^{-1}$ (*92*)], the electron-transfer rate would have to be 70 times faster than the previous estimate of $\approx 10^6$ s$^{-1}$ (*12*, *90*).

Kinetic measurements provide a free energy for the reaction $Q_A^-Q_B^- + e^- + H^+ \rightarrow Q_AQ_BH^-$ of $-70 \pm 10$ meV at pH 7.5 (*89*), equivalent to a $\Delta G$ of $-100$ meV at pH 7. $\Delta G$ for $Q_A^-Q_BH \rightarrow Q_AQ_BH^-$ would then be $-250$ meV. The value calculated here is $-405$ meV, significantly more favorable. One possible problem is that the $E_m$ for $Q_BH^-$ relies on the $E_{m,sol}$ for $Q^-/Q^{-2}$. A higher energy of $Q^{-2}$ would raise that of $Q_AQ_BH^-$, reducing the calculated $\Delta G$ between $Q_A^-Q_B^-$ and $Q_AQ_BH^-$.

Given the high energy of the $Q_AQ_B^{-2}$ state, the free-energy difference between $Q_A^-Q_B^-$ and $Q_AQ_B^{-2}$ states is not measurable. The $E_m$ ($Q_B^-/Q_B^{-2}$) has been estimated to be more negative than $-240$ mV (C. A. Wraight, personal communication). The calculated value is $-464$ mV. An experimental p$K_a$ of >10.7 was obtained for binding a proton to $Q_B^{-2}$ in the state $Q_A^-Q_B^{-2}$ (*36*, *93*). The calculated value is 17.3. The p$K_a$ for $Q_AQ_BH^- + H^+ \rightarrow Q_AQ_BH_2$ was estimated to be $8.5 \pm 0.3$ from the steady-state proton uptake by $Q_B^{-2}$ (*89*, *92*). This corresponds to a reaction free energy of $-90 \pm 18$ meV at pH 7, in reasonable agreement with the calculated value of $-60$ meV.

## DISCUSSION

*Quinone Energies in the Three RC-Binding Sites.* In RCs of *Rb. sphaeroides* and *Rps. viridis*, three quinone-binding sites are found in various X-ray structures (*21*, *82*, *94*, *95*). The two quinones symmetrically arranged around the non-heme iron are clearly identified with functionally well-characterized $Q_A$ and $Q_B$ (*1*, *2*, *12*). $Q_A$ is the first quinone reduced, accepting an electron from the bacteriopheophytin in $\approx$150 ns (*96*). On two turnovers, $Q_A^-$ reduces $Q_B$ and then the $Q_B$ semiquinone with rates of $\approx$100 $\mu$s (*14*, *97*) prior to $Q_B$ leaving the protein as dihydroquinone (*17*). The role of the distal quinone site is not yet clear (*21*−*24*, *26*). MCCE has been used here to see how the RC structure influences the free energy of the quinone redox states so that ubiquinone can carry out its different functions in these sites (Figure 4 and Table 2). Different states are stabilized so that in each site the appropriate reactions are energetically accessible. In addition, each quinone species has a different affinity for each binding site. For example, quinone comes and goes in $Q_B$ and $Q_{BD}$ sites but never leaves the $Q_A$ site. The connection between the stabilization of a redox state and the relative affinity of different redox states shows why the semiquinone does not bind to the $Q_{BD}$ site but does not leave the $Q_B$ site. (Figure 2) (*98*).

*$Q_A$.* $Q_A$, is reduced by the bacteriopheophytin anion, which only lives for a few nanoseconds. Thus, this quinone never dissociates so that it is always ready to react (*74*, *99*). $Q_A$ serves as a single-electron acceptor cycling between $Q_A$ and $Q_A^-$ without binding protons. The MCCE calculations show that the $Q_A$ site stabilizes only the semiquinone (Table 2). The calculated $E_m$, made assuming an $E_{m,sol}$ for ubiquinone in water of $-145$ mV, is $-37$ mV, in good agreement with the measured value of $\approx -60$ mV (*75*, *83*). The protein interacts weakly with a proton on either carbonyl. The free energy of proton binding is 89 meV less favorable in the $Q_A$ site than in solution, lowering the semiquinone p$K_a'$ from 4.9 to 3.4.

*$Q_B$.* $Q_B$ has been measured to be 20 times more weakly bound than $Q_A$ (*74*, *99*). This is acceptable because $Q_A^-$ lives for hundreds of milliseconds; therefore, $Q_B$ has time to bind to an empty site before $P^+Q_A^-$ returns to the ground state, which would waste the energy of the absorbed photon. $Q_B$ cycles through the $Q_B$, $Q_B^-$, $Q_BH$, $Q_BH^-$, and $Q_BH_2$ states during turnover, alternating reduction and protonation reactions. The proximal $Q_B$ site stabilizes the anionic states $Q_B^-$ and $Q_BH^-$ and interacts weakly or slightly unfavorably with the protonated neutral states $Q_BH$ and $Q_BH_2$. An important requirement for RC function is that $Q_A^-$ can reduce both quinone and semiquinone species within the millisecond lifetime of $Q_A^-$. Despite the $c_2$ symmetry of $Q_A$ and $Q_B$ sites in the protein, the $Q_B$ site stabilizes the semiquinone somewhat more that the $Q_A$ site, in large part because of the larger positive potential from the backbone dipoles in the proximal $Q_B$ site. The free energy for the first electron transfer is modest, $\approx -70$ meV experimentally (*86*−*88*) and $-30$ meV here; therefore, $Q_B^-$ is not deeply trapped. This allows the electron to return to $P^+$ reforming the ground state via reduction of $Q_A$ with a half-time of $\approx$1 s if a second electron is not delivered to $Q_B$. The $Q_B$ site stabilizes $Q_BH$ a little relative to Q in solution (Figure 4), making the $\Delta G$ between $Q_B^-$ and $Q_BH$ larger than it is in solution. However, the site destabilizes $Q_B^{-2}$ more; therefore, $Q_BH$ and not the dianion is the intermediate for the second reduction of $Q_B$, in agreement with previous suggestions (*90*, *100*). If the semiquinone species were to leave the $Q_B$ site before the second electron is delivered from $Q_A^-$, the energy of the photon would be lost. The $-140$ meV stabilization of $Q_B^-$ and $-110$ meV stabilization of $Q_BH^-$ ensures that these will bind more tightly to the $Q_B$ site then does the quinone. The $Q_B$ site stabilizes anions without a strong penalty for proton binding. This allows a favorable free energy for electron transfer from $Q_A^-$ to $Q_BH$ to form $Q_BH^-$. There is a modest, 50 meV, destabilization of $Q_BH_2$. This puts the energy of $Q_BH_2$ below that of $Q_BH^-$ but above that of $QH_2$ in solution, yielding favorable proton binding to $Q_BH^-$ but weak binding to the $Q_B$ pocket.

*$Q_{BD}$.* RC crystal structures have shown that ubiquinone binds in several positions in the $Q_B$ site (*95*). X-ray crystal structures were compared of RCs frozen in the light and dark. In the dark-adapted structures, where the quinone was assumed to be oxidized, it was found in the outer distal site (*21*). In the light-adapted structure, where the state was assumed to be $P^+Q_B^-$, the quinone is in the proximal site. The distal headgroup moves $\approx$5 Å out of the protein into a location overlapping the tail of a proximal quinone. In addition, the two positions differ by a 180° rotation around the isoprene tail. Prior kinetic data had shown that the electron transfer from $Q_A^-$ to $Q_B$ is gated by a conformational change (*101*). The motion from proximal to distal binding

sites was proposed as a good candidate for this rate-determining step (*21*). However, several more recent experiments have cast doubt on this hypothesis. Recent time-resolved crystallography in *Rps. viridis* (*26*) shows that only the proximal site is occupied at room temperature in ground and $P^+Q_B^-$ states of RCs that are undergoing turnover. This agrees with FTIR studies that there are no changes in the quinone position in active *Rb. sphaeroides* RCs (*22*, *23*). Likewise, the kinetic studies show that the tail has little effect on the electron transfer from $Q_A^-$ to $Q_B$, unexpected if the quinone needs to undergo rotation and translation in the rate-determining step (*15*, *24*, *99*). The quinone position in crystals is sensitive to mutation (*102*), temperature, and cryoprotectant (*103*). Computational analysis has explored the transition from the proximal to distal position showing there is a little barrier to movement without (*40*, *41*) and a large barrier to movement with (*39*) the 180° rotation. The protonation of the acidic cluster changes the relative affinity of the proximal and distal sites (*40*, *41*). In addition, as is found here (Appendix I in the Supporting Information), the proton uptake on $Q_B$ reduction depends on the quinone location (*27*).

MCCE analysis shows that the distal $Q_B$ site ($Q_{BD}$) destabilizes all anionic quinone species while stabilizing the protonated neutral states (Figure 3). Both $\Delta G_{pol}$ and $\Delta G_{res}$ are significantly less favorable than they are in the $Q_B$ site. Reduction of $Q_{BD}$ to $Q_{BD}^-$ is ≈120 meV less favorable than it is in solution and 260 meV less favorable than in the proximal $Q_B$ site. Thus, $Q_A$ could not reduce $Q_{BD}$; therefore, it is highly unlikely that electron transfer could occur to a quinone bound there. This is in agreement with prior calculations of RCs *Rps. viridis* (*44*). Earlier calculations on *Rb. sphaeroides* RCs show a 210 meV difference between reduction at the two sites, in good agreement with the values found here (*38*, *46*). However, the neutral, protonated quinone species $Q_{BD}H$ and $Q_{BD}H_2$ are stabilized in the distal binding site. Thus, the dihydroquinone will be bound ≈3 times more tightly than the quinone to the distal site. It has been suggested that dihydroquinone, reduced during data collection, is the species found in the RC crystal $Q_{BD}$ site (*55*, *94*).

*Comparisons with Earlier Experimental and Computational Studies.* The values have been presented to the nearest millivolt here as an aid for tracking the connections between numbers in different tables. However, neither the calculations nor the experimental data to which it is compared are known with this certainty. The uncertainty of the Monte Carlo sampling for this model of the RCs is less than 5 mV. MCCE analysis of benchmark $E_m$ (*63*) and p$K_a$ (*54*) values show that >90% of the residues have an error of less than 60 mV or 1 pH unit. The calculations are sensitive to the starting crystal structures, parameters, and conformers (*53*). MCCE does not allow the backbone to change conformation, and only limited side-chain positions are sampled.

*Ionization of the Acidic Cluster.* Perhaps the most difficult part of the simulation to define is the protonation state of the acidic cluster near $Q_B$, including GluL212, AspL213, AspL210, and GluH173 (Appendix I in the Supporting Information). Their ionization states when the quinone is in the ground and $Q_B^-$ states have been the subject of many experimental (*1*, *2*, *33*) and computational (*37*, *38*, *45*, *46*) studies. Experiment, especially FTIR measurements, have indicated that a partially deprotonated GluL212 becomes protonated when $Q_B$ is reduced (*35*, *104*, *105*). Simulations find that GluL212 and AspL213 are strongly coupled. Some calculations find that GluL212 is ionized (*38*, *43*, *45*, *46*), and others find that AspL213 is ionized (*37*, *41*), In calculations, the pair usually have a net charge of −1 as they do here. When $Q_B$ is reduced, GluL212 and AspL213 are always neutral, retaining a cluster net charge of −1.

In the simulations starting with 1AIJ presented here, when $Q_B$ is oxidized, GluL212 is ionized (Appendix I in the Supporting Information). In parallel, in MCCE calculations carried out with 1M3X (*106*), GluL212 is neutral and AspL213 is ionized in the ground state (data not shown). This ease of shifting of the order of acid ionization arises because these two acids interact strongly; therefore, only one can be ionized. They have similar p$K_a$ values in the absence of the interaction with each other; therefore, their ionization free energy is similar. Modest changes in the structure cause one or the other to be ionized first, keeping the other neutral to high pH. However, the $E_m$ for $Q_B$ differs by only 10 mV, and the proton uptake is the same (0.7 $H^+/e^-$) in the simulations on 1AIJ and 1M3X. This is a result of the free energy of the reactant microstates, with $Q_B$/L212$^-$/L213H and $Q_B$/L212H/L213$^-$ being very close together. The product state is always $Q_B^-$/L212H/L213H. This explains why the free energy of electron transfer from $Q_A^-$ to $Q_B$ in our earlier calculations, where GluL212 was protonated and AspL213 was ionized in the ground state, differ by only ≈40 meV from those presented here (*37*). Similar clusters of acidic residues with coupled protonation are also found in bacteriorhodopsin (*65*).

*Importance of the Membrane.* While most measurements on bacterial RCs are carried out with detergent-solubilized protein, RCs function *in vivo* embedded in the cell membrane. The reported reaction $E_m$ and p$K_a$ values are somewhat dependent on the measurement conditions. For example, quinone $E_m$ values are lower in chromatophores than in the isolated RC (*107*). In contrast, preliminary calculations show that addition of a low dielectric slab to simulate the membrane (*108*) raises both the $Q_A$ and $Q_B$ semiquinone $E_m$ values because there are more basic residues further from the quinones and more acidic residues nearby. Without the low dielectric slab, the surrounding water screens the influence of the more distant positively charged groups. Experiments show addition of a few bound cardiolipin molecules can lower the $Q_A/Q_A^-$ $E_m$ by −30 mV; therefore, at least some of the difference found in membranes may be due to the binding of specific lipids rather than the impact of dielectric screening by the membrane (*109*). Measurements provide a $\Delta G$ for electron transfer from $Q_A^-$ to $Q_B$ of ≈65 and ≈75 meV in chromatophores when P is neutral (*110*). In chromatophores, the reaction is 45 meV more favorable when P is oxidized, indicating $P^+$ stabilizes $Q_B^-$ more than $Q_A^-$ (*110*). In contrast, the $\Delta G$ for electron transfer from $Q_A^-$ to $Q_B$ is relatively independent of the ionization state of P in isolated RCs (*87*, *111*). The quinone p$K_a$ values can also depend on the environment. Thus, an experimental estimate for the p$K_a$ of $Q^- + H^+ \rightarrow QH$ is 4.5 in detergent-solubilized RCs (*90*) and 6 in chromatophores (*107*).

*Role of SerL223.* The position of the hydroxyl on SerL223 depends on the initial proton distribution on the acidic cluster in the $Q_B$ site. When AspL213 is neutral, as in these 1AIJ

calculations, two hydroxyl positions are found in Monte Carlo sampling; therefore, in the ensemble, some SerL223 donate a hydrogen bond to and others accept a hydrogen bond from the neutral $Q_B$ (Table 4). However, if AspL213 is ionized when $Q_B$ is neutral, as it is in the 1M3X calculations, the hydroxyl of SerL223 points to the Asp, away from $Q_B$. In both cases, when $Q_B$ is reduced, SerL223 serves as a hydrogen-bond donor to the anionic semiquinone. The results presented here are in good agreement with a computational analysis that focused on the importance of SerL223 (*81*). The results presented here reaffirm the dependence of the Ser hydroxyl orientation on the charge of AspL213 and the approximate magnitude of the change in $Q_B$ $E_m$ if the Ser is fixed in one position or the other. If AspL213 is neutral when $Q_B$ is oxidized, the conformations with different proton positions are close in energy and small changes in structure or fitting parameters could easily change the distribution. Thus, it seems likely that the Ser hydroxyl reorientation provides a significant barrier to electron transfer from $Q_A^-$ to $Q_B$ only if AspL213 and not GluL212 is the member of the acidic cluster that is ionized when $Q_B$ is oxidized.

*Pathway of Proton Transfer to $Q_B$.* Site-directed mutagenesis suggests that the first proton is transferred to the carbonyl from AspL213 via SerL223 and that the second proton is transferred to oxygen near HisL190 through a pathway involving GluL212 (*29*, *112*, *113*). This is consistent with the first quinone proton being bound to the carbonyl near the SerL223 (Table 4). However, in these calculations, the proton on the carbonyl hydrogen-bonded to HisL190, pointing away from the His NE2 hydrogen, and the non-heme iron is found in 30% of $Q_BH$ (Figure 5). This position has weak but favorable Lennard−Jones interactions with both HisL190 and the non-heme iron. It may be that this proton can compete with protonation of the other carbonyl in equilibrium simulations but would not be seen in RCs because protonation from the Ser is much faster. It also maybe that the favorable nonelectrostatic interactions are over-estimated.

*Importance of $E_{m,sol}$.* The calculated $E_m$ values versus S.H.E., quinone p$K_a$ values, and reaction $\Delta G$ values (Table 5) depend on the reference $E_{m,sol}$ and p$K_{a,sol}$ (*63*). As described in the Materials and Methods, aqueous $E_m$ and p$K_a$ values for ubiquionone have an uncomfortable number of uncertainties. Different errors in $E_{m,sol}$ for different half-reactions will yield errors in calculated $\Delta G$ values. For example, the calculated free-energy change for $Q_A^-Q_BH \rightarrow Q_AQ_BH^-$ is 150 meV more favorable than that estimated from the measurements (Figure 7) (*89*). The calculated $\Delta G$ for the reaction relies on p$K_{a,sol}$ for $Q^{-2}$ and $E_{m,sol}$ for the reduction of the semiquinone, as well as the calculated shift of the energy in the protein, $\Delta\Delta G_{protein}$. Errors in any of these terms will change the results.

Different analyses of RC electrochemistry have used different values for $E_{m,sol}$. For example, Knapp and coworkers (*38*) use −360 mV for the $E_{m,sol}$ for $Q/Q^-$ in DMF, a noninteracting reference solvent. In contrast, we prefer that all solution values are estimated in aqueous solution, because continuum calculations are optimized to determine transfers from water to the protein. Thus, the aqueous $E_{m,sol}$ of −145 mV, used here, is 215 mV more positive than that found in DMF. The $E_m$ values from ref *38* are reported to be more negative than those obtained here. However, their shifts in $E_m$ because of the protein actually favor $Q_A$ or $Q_B$ reduction to semiquinone by ≈100 meV more than those found here. The $\Delta G$ for the electron transfer between the two quinones is a value that is independent of $E_{m,sol}$. Calculated values at pH 7 range from −65 meV (*37*) to −60 meV (*38*) to −30 meV here. This is a remarkable agreement considering the complexity of these calculations.

## ACKNOWLEDGMENT

We thank Colin Wraight for discussions of quinone electrochemistry. We gratefully acknowledge the financial support of NSF MCB 0212696 and CREST NSF Cooperative Agreement HRD 0206162.

## SUPPORTING INFORMATION AVAILABLE

Appendix I, protonation and ionization states of selected residues at pH 7 calculated by MCCE calculation here and from previous calculations and experiments. This material is available free of charge via the Internet at http://pubs.acs.org.

## REFERENCES

1. Wraight, C. A. (2004) Proton and electron transfer in the acceptor quinone complex of photosynthetic reaction centers from *Rhodobacter sphaeroides*, *Front. Biosci. 9*, 309−337.
2. Paddock, M. L., Feher, G., and Okamura, M. Y. (2003) Proton-transfer pathways and mechanism in bacterial reaction centers, *FEBS Lett. 555*, 45−50.
3. Rutherford, A. W., and Faller, P. (2001) The heart of photosynthesis in glorious 3D, *Trends Biochem. Sci. 26*, 341−344.
4. Fromme, P., Jordan, P., and Krauss, N. (2001) Structure of photosystem I, *Biochim. Biophys. Acta 1507*, 5−31.
5. Hunte, C., Palsdottir, H., and Trumpower, B. L. (2003) Proton-motive pathways and mechanisms in the cytochrome $bc_1$ complex, *FEBS Lett. 545*, 39−46.
6. Cramer, W. A., Zhang, H., Yan, J., Kurisu, G., and Smith, J. L. (2004) Evolution of photosynthesis: Time-independent structure of the cytochrome $b_6f$ complex, *Biochemistry 43*, 5921−5929.
7. Stroebel, D., Choquet, Y., Popot, J. L., and Picot, D. (2003) An atypical haem in the cytochrome $b_6f$ complex, *Nature 426*, 413−418.
8. Kurisu, G., Zhang, H., Smith, J. L., and Cramer, W. A. (2003) Structure of the cytochrome $b_6f$ complex of oxygenic photosynthesis: Tuning the cavity, *Science 302*, 1009−1014.
9. Cecchini, G., Maklashina, E., Yankovskaya, V., Iverson, T. M., and Iwata, S. (2003) Variation in proton donor/acceptor pathways in succinate:quinone oxidoreductases, *FEBS Lett. 545*, 31−38.
10. Lancaster, C. R. (2003) Wolinella succinogenes quinol:fumarate reductase and its comparison to *E. coli* succinate:quinone reductase, *FEBS Lett. 555*, 21−28.
11. Rich, P. R., and Bendall, D. S. (1979) A mechanism for the reduction of cytochromes by quinols in solution and its relevance to biological electron transfer reactions, *FEBS Lett. 105*, 189−194.
12. Okamura, M. Y., Paddock, M. L., Graige, M. S., and Feher, G. (2000) Proton and electron transfer in bacterial reaction centers, *Biochim. Biophys. Acta 1458*, 148−163.
13. Gunner, M. R., and Alexov, E. (2000) A pragmatic approach to structure based calculation of coupled proton and electron transfer in proteins, *Biochim. Biophys. Acta 1458*, 63−87.
14. Graige, M. S., Feher, G., and Okamura, M. Y. (1998) Conformational gating of the electron-transfer reaction $Q_A^-Q_B \rightarrow Q_AQ_B^-$ in bacterial reaction centers of *Rhodobacter sphaeroides* determined by a driving force assay, *Proc. Natl. Acad. Sci. U.S.A. 95*, 11679−11684.
15. Li, J., Takahashi, E., and Gunner, M. R. (2000) $-\Delta G_{AB}^\circ$ and pH dependence on the electron transfer from $P^+Q_A^-Q_B$ to $P^+Q_AQ_B^-$ in *Rhodobacter sphaeroides* reaction centers, *Biochemistry 39*, 7445−7454.

16. Graige, M. S., Paddock, M. L., Bruce, J. M., Feher, G., and Okamura, M. Y. (1996) Mechanism of proton-coupled electron transfer for quinone ($Q_B$) reduction in reaction centers of *Rb. sphaeroides*, *J. Am. Chem. Soc. 118*, 9005−9016.
17. McPherson, P. H., Okamura, M. Y., and Feher, G. (1990) Electron transfer from the reaction center of *Rb. sphaeroides* to the quinone pool: Doubly reduced $Q_B$ leaves the reaction center, *Biochim. Biophys. Acta 1016*, 289−292.
18. Wraight, C. A. (1979) Electron acceptors of bacterial photosynthetic reaction centers II. $H^+$ binding coupled to secondary electron transfer in the quinone acceptor complex, *Biochim. Biophys. Acta 548*, 309−327.
19. Diner, B. A., Schenck, C. C., and DeVitry, C. (1984) Effect of inhibitors, redox state, and isoprenoid chain length on the affinity of ubiquinone for the secondary acceptor binding site in the reaction centers of photosynthetic bacteria, *Biochim. Biophys. Acta 766*, 9−20.
20. Lancaster, C. R. D. (1998) Ubiquinone reduction and protonation in photosynthetic reaction centres from *Rhodopseudomonas viridis*: X-ray strucutres and their functional implications, *Biochim. Biophys. Acta 1365*, 143−150.
21. Stowell, M. H. B., McPhillips, T. M., Rees, D. C., Soltis, S. M., Abresch, E., and Feher, G. (1997) Light-induced structural changes in photosynthetic reaction center: Implications for mechanism of electron−proton transfer, *Science 276*, 812−816.
22. Remy, A., and Gerwert, K. (2003) Coupling of light-induced electron transfer to proton uptake in photosynthesis, *Nat. Struct. Biol. 10*, 637−644.
23. Breton, J., Boullais, C., Mioskowski, C., Sebban, P., Bacious, L., and Nabedryk, E. (2002) Vibrational spectroscopy favors a unique $Q_B$ binding site at the proximal position in wild-type reaction centers and in the Pro-L209 → Tyr mutant from *Rhodobacter sphaeroides*, *Biochemistry 41*, 12921−12927.
24. Xu, Q., Baciou, L., Sebban, P., and Gunner, M. R. (2002) Exploring the energy landscape for $Q_A^-$ to $Q_B$ electron transfer in bacterial photosynthetic reaction centers: Effect of substrate position and tail length on the conformational gating step, *Biochemistry 41*, 10021−10025.
25. Breton, J. (2004) Absence of large-scale displacement of quinone $Q_B$ in bacterial photosynthetic reaction centers, *Biochemistry 43*, 3318−3326.
26. Pokkuluri, P. R., Laible, P. D., Crawford, A. E., Mayfield, J. F., Yousef, M. A., Ginell, S. L., Hanson, D. K., and Schiffer, M. (2004) Temperature and cryoprotectant influence secondary quinone binding position in bacterial reaction centers, *FEBS Lett. 570*, 171−174.
27. Taly, A., Sebban, P., Smith, J. C., and Ullmann, G. M. (2003) The position of $Q_B$ in the photosynthetic reaction center depends on pH: A theoretical analysis of the proton uptake upon $Q_B$ reduction, *Biophys. J. 84*, 2090−2098.
28. Paddock, M. L., Rongey, S. H., Feher, G., and Okamura, M. Y. (1989) Pathway of proton transfer in bacterial reaction centers: Replacement of glutamic acid 212 in the L subunit by glutamine inhibits quinone (secondary acceptor) turnover, *Proc. Natl. Acad. Sci. U.S.A. 86*, 6602−6606.
29. Paddock, M. L., McPherson, P. H., Feher, G., and Okamura, M. Y. (1990) Pathway of proton transfer in bacterial reaction centers: Replacement of serine-L223 by alanine inhibits electron and proton transfers associated with reduction of quinone to dihydroquinone, *Proc. Natl. Acad. Sci. U.S.A. 87*, 6803−6807.
30. Rongey, S. H., Paddock, M. L., Feher, G., and Okamura, M. Y. (1993) Pathway of proton transfer in bacterial reaction centers: Second-site mutation Asn-M44 → Asp restores electron and proton transfer in reaction centers form the photosynthetically deficient Asp-L213 → Asn mutant of *Rhodobacter sphaeroides*, *Proc. Natl. Acad. Sci. 90*, 1325−1329.
31. Paddock, M. L., Rongey, S. H., McPherson, P. H., Juth, A., Feher, G., and Okamura, M. Y. (1994) Pathway of proton transfer in bacterial reaction centers: Role of aspartate-L213 in proton transfers associated with reduction of quinone to dihydroquinone, *Biochemistry 33*, 734−745.
32. Maroti, P., Hanson, D. K., Schiffer, M., and Sebban, P. (1995) Long-range electrostatic interaction in the bacterial photosynthetic reaction centre, *Nat. Struct. Biol. 2*, 1057−1059.
33. Sebban, P., Maroti, P., Schiffer, M., and Hanson, D. K. (1995) Electrostatic dominoes: Long distance propagation of mutational effects in photosynthetic reaction centers of *Rhodobacter capsulatus*, *Biochemistry 34*, 8390−8397.
34. Paddock, M. L., Adelroth, P., Chang, C., Abresch, E. C., Feher, G., and Okamura, M. Y. (2001) Identification of the proton pathway in bacterial reaction centers: Cooperation obetween Asp-M17 and Asp-L210 facilitates proton transfer to the secondary quinone ($Q_B$), *Biochemistry 40*, 6893−6902.
35. Nabedryk, E., Breton, J., Okamura, M. Y., and Paddock, M. L. (2001) Simultaneous replacement of Asp-L210 and Asp-M17 with Asn increases proton uptake by Glu-L212 upon first electron transfer to $Q_B$ in reaction centers from *Rhodobacter sphaeroides*, *Biochemistry 40*, 13826−13832.
36. Takahashi, E., and Wraight, C. A. (1992) Proton and electron transfer in the acceptor quinone complex of *Rhodobacter sphaeroides* reaction centers: Characterization of site-directed mutants of the two ionizable residues, Glu L212 and Asp L213, in the $Q_B$ binding site, *Biochemistry 31*, 855−866.
37. Alexov, E., and Gunner, M. (1999) Calculated protein and proton motions coupled to electron transfer: Electron transfer from $Q_A^-$ to $Q_B$ in bacterial photosynthetic RCs, *Biochemistry 38*, 8253−8270.
38. Ishikita, H., Morra, G., and Knapp, E. W. (2003) Redox potential of quinones in photosynthetic reaction centers from *Rhodobacter sphaeroides*: Dependence on protonation of Glu-L212 and Asp-L213, *Biochemistry 42*, 3882−3892.
39. Zachariae, U., and Lancaster, C. R. (2001) Proton uptake associated with the reduction of the primary quinone $Q_A$ influences the binding site of the secondary quinone $Q_B$ in *Rhodopseudomonas viridis* photosynthetic reaction centers, *Biochim. Biophys. Acta 1505*, 280−290.
40. Walden, S. E., and Wheeler, R. A. (2002) Protein conformational gate controlling binding site preference and migration for ubiquinone-B in the photosynthetic reactin center of *Rhodobacter sphaeroides*, *J. Phys. Chem. B 106*, 3001−3006.
41. Grafton, A. K., and Wheeler, R. A. (1999) Amino acid protonation states determine binding sites of the secondary ubiquinone and its anion in the *Rhodobacter spaeroides* photosynthetic reaction center, *J. Phys. Chem. 103*, 5380−5387.
42. Schutz, C. N., and Warshel, A. (2001) What are the "dielectric constants" of proteins and how to validate electrostatic models? *Proteins 44*, 400−417.
43. Lancaster, C. R. D., Michel, H., Honig, B., and Gunner, M. R. (1996) Calculated coupling of electron and proton transfer in the photosynthetic reaction center of *Rhodopseudomonas viridis*, *Biophys. J. 70*, 2469−2492.
44. Rabenstein, B., Ullmann, G. M., and Knapp, E.-W. (1998) Energetics of electron-transfer and protonation reactions of the quinones in the photosynthetic reaction center of *Rhodopseudonas viridis*, *Biochemistry 37*, 2488−2495.
45. Beroza, P., Fredkin, D. R., Okamura, M. Y., and Feher, R. (1995) Electrostatic calculations of amino acid titration electron transfer, $Q^-_AQ_B \rightarrow Q_AQ_B^-$, in the reaction center, *Biophys. J. 68*, 2233−2250.
46. Rabenstein, B., Ullmann, G. M., and Knapp, E. W. (2000) Electron transfer between the quinones in the photosynthetic reaction center and its coupling to conformational changes, *Biochemistry 39*, 10487−10496.
47. Alexov, E., Miksovska, J., Baciou, L., Schiffer, M., Hanson, D., Sebban, P., and Gunner, M. R. (2000) Modeling the effects of mutations on the free energy of the first electron transfer from $Q_A^-$ to $Q_B$ in photosynthetic reaction centers, *Biochemistry 39*, 5940−5952.
48. Simonson, T. (2001) Macromolecular electrostatics: Continuum models and their growing pains, *Curr. Opin. Struct. Biol. 11*, 243−252.
49. Bashford, D., and Karplus, M. (1990) The p$K_a$'s of ionizable groups in proteins: Atomic detail from a continuum electrostatic model, *Biochemistry 29*, 10219−10225.
50. Yang, A.-S., Gunner, M. R., Sampogna, R., Sharp, K., and Honig, B. (1993) On the calculation of p$K_a$'s in proteins, *Proteins 15*, 252−265.
51. Beroza, P., and Case, D. (1996) Including side chain flexibility in continuum electrostatic calculations of protein titration, *J. Phys. Chem. 100*, 20156−20163.
52. You, T. J., and Bashford, D. (1995) Conformation and hydrogen ion titration of proteins: A continuum electrostatic model with conformational flexibility, *Biophys. J. 69*, 1721−1733.
53. Alexov, E. G., and Gunner, M. R. (1997) Incorporating protein conformational flexibility into the calculation of pH-dependent protein properties, *Biophys. J. 72*, 2075−2093.

54. Georgescu, R. E., Alexov, E. G., and Gunner, M. R. (2002) Combining conformational flexibility and continuum electrostatics for calculating p$K_a$'s in proteins, *Biophys J. 83*, 1731−1748.
55. Fritzsch, G., Koepke, J., Diem, R., Kuglstatter, A., and Baciou, L. (2002) Charge separation induces conformational changes in the photosynthetic reaction centre of purple bacteria, *Acta Crystallogr., Sect. D 58*, 1660−1663.
56. Sridharan, S., Nicholls, A., and Honig, B. (1992) A new vertex algorithm to calculate solvent accessible surface areas, *Biophys. J. 61*, A174.
57. Bharadwaj, R., Windemuth, A., Sridharan, S., Honig, B., and Nicholls, A. (1995) The fast multipole boundary element method for molecular electrostatics: An optimal approach for large systems, *J. Comp. Chem. 16*, 898−913.
58. Parson, W. W., Chu, Z.-T., and Warshel, A. (1990) Electrostatic control of charge separation in bacterial photosynthesis, *Biochim. Biophys. Acta 1017*, 251−272.
59. Sitkoff, D., Sharp, K. A., and Honig, B. (1994) Accurate calculation of hydration free energies using macroscopic solvent models, *J. Phys. Chem. 98*, 1978−1988.
60. Nicholls, A., and Honig, B. (1991) A rapid finite difference algorithm utilizing successive over-relaxation to solve the Poisson−Boltzmann equation, *J. Comp. Chem. 12*, 435−445.
61. Rocchia, W., Alexov, E., and Honig, B. (2001) Extending the applicability of the nonlinear Poisson−Boltzmann Equation: Multiple dielectric constants and multivalent ions, *J. Phys. Chem. B 105*, 6507−6514.
62. Gilson, M. K., and Honig, B. (1988) Calculation of the total electrostatic energy of a macromolecular system: solation energies, binding energies, and conformational analysis, *Proteins 4*, 7−18.
63. Mao, J., Hauser, K., and Gunner, M. R. (2003) How cytochromes with different folds control heme redox potentials, *Biochemistry 42*, 9829−9840.
64. Beroza, P., Fredkin, D. R., Okamura, M. Y., and Feher, G. (1991) Protonation of interacting residues in a protein by a Monte Carlo method: Application to lysozyme and the photosynthetic reaction center of *Rhodobacter sphaeroides*, *Proc. Natl. Acad. Sci. U.S.A. 88*, 5804−5808.
65. Song, Y., Mao, J., and Gunner, M. R. (2003) Calculation of proton transfers in *Bacteriorhodopsin* bR and M intermediates, *Biochemistry 42*, 9875−9888.
66. Rich, P. R. (2004) The quinone chemistry of bc complexes, *Biochim. Biophys. Acta 1658*, 165−171.
67. Swallow, A. J. (1982) in *Function of Quinones in Energy Conserving Systems* (Trumpower, B. L., Ed.) pp 59−72, Academic Press, New York.
68. Prince, R. C., Dutton, P. L., and Bruce, J. M. (1983) Electrochemistry of ubiquinones, *FEBS 160*, 273−276.
69. Wraight, C. A. (1998) in *Proceedings of the 11th International Photosynthesis Congress* (Garab, G., Ed.) pp 693−698, Kluwer, Dordrecht, The Netherlands.
70. Morrison, L. E., Schelhorn, J. E., Cotton, T. E., Bering, C. L., and Loach, P. A. (1982) in *Function of Quinones in Energy Conserving Systems* (Trumpower, B. L., Ed.) pp 35−58, Academic Press, New York.
71. Gordillo, G. J., and Schiffrin, D. J. (2000) The electrochemistry of ubiquinone-10 in a phospholipid model membrane, *Faraday Discuss. 116*, 89−107.
72. Bishop, C. A., and Tong, L. K. J. (1965) Equilibria of substituted semiquinones at high pH, *J. Am. Chem. Soc. 18*, 501−505.
73. van Gunsteren, W. F., Daura, X., and Mark, A. E. (2002) Computation of free energy, *Helv. Chim. Acta 85*, 3113−3129.
74. Warncke, K., and Dutton, P. L. (1993) Influence of $Q_A$ site redox cofactor structure on equilibrium binding, in situ electrochemistry, and electron-transfer performance in the photosynthetic reaction center protein, *Biochemistry 32*, 4769−4779.
75. Rutherford, A. W., and Evans, M. C. W. (1980) Direct measurement of the redox potential of the primary and secondary quinone electron acceptors in *Rhodopseudomonas sphaeroides* (wild-type) by EPR spectrometry, *FEBS Lett. 110*, 257−261.
76. Gunner, M. R., Saleh, M., Cross, E., ud-Doula, A., and Wise, M. (2000) Backbone dipoles generate positive potentials in all proteins. Origins and implications of the effect, *Biophys. J. 78*, 1126−1144.
77. Lancaster, C. R. (2003) The role of electrostatics in proton-conducting membrane protein complexes, *FEBS Lett. 545*, 52−60.
78. Kleinfeld, D., Okamura, M. Y., and Feher, G. (1984) Electron-transfer kinetics in photosynthetic reaction centers cooled to cryogenic temperatures in the charge separated state: Evidence for light-induced structural changes, *Biochemistry 23*, 5780−5786.
79. Xu, Q., and Gunner, M. R. (2001) Trapping conformational intermediate states in the reaction center protein from photosynthetic bacteria, *Biochemistry 40*, 3232−3241.
80. Bockris, J. O. M., and Reddy, A. K. N. (1973) *Modern Electrochemistry*, Vol. 1, Plenum, New York.
81. Ishikita, H., and Knapp, E.-W. (2004) Variation of Ser-L223 hydrogen bonding with the $Q_B$ redox state in reaction centers from *Rhodobacter sphaeroides*, *J. Am. Chem. Soc. 126*, 8059−8064.
82. Lancaster, R., and Michel, H. (1997) The coupling of light-induced electron transfer and proton uptake as derived from crystal structures of reaction centers from *Rhodopseudomonas viridis* modified at the binding site of the secondary quinone, $Q_B$, *Structure 5*, 1339−1359.
83. Dutton, P. L., Leigh, J. S., and Wraight, C. A. (1973) Direct measurement of the midpoint potential of the primary electron acceptor in *Rhodopsuedomonas sphaeroides* in situ and in the isolated state: Some relationships with pH and *o*-phenathroline, *FEBS Lett. 36*, 169−173.
84. Gunner, M. R., Robertson, D. E., and Dutton, P. L. (1986) Kinetic studies on the reaction center protein from *Rhodopseudomonas sphaeroides*: The temperature and free energy dependence of electron transfer between various quinones in the $Q_A$ site and the oxidized bacteriochlorophyll dimer, *J. Phys. Chem. 90*, 3783−3795.
85. Kalman, L., and Maroti, P. (1997) Conformation-activated protonation in reaction centers of the photosynthetic bacterium *Rodobacter sphaeroides*, *Biochemistry 36*, 15269−15276.
86. Mancino, L. J., Dean, D. P., and Blankenship, R. E. (1984) Kinetics and thermodynamics of the $P870^+Q_A^- \rightarrow P870^+Q_B^-$ reaction in isolated reaction centers from the photosynthetic bacterium *Rhodopseudomonas sphaeroides*, *Biochim. Biophys. Acta 764*, 46−54.
87. Kleinfeld, D., Okamura, M. Y., and Feher, G. (1984) Electron transfer in reaction centers of *Rhodopseudomonas sphaeroides*: I. Determination of the charge recombination pathway of $D^+Q_AQ_B^-$ and free energy and kinetic relations between $Q_A^-Q_B$ and $Q_AQ_B^-$, *Biochim. Biophys. Acta 766*, 126−140.
88. McPherson, P. H., Okamura, M. Y., and Feher, G. (1988) Light-induced proton uptake by photosynthetic reaction centers from *Rhodobacter sphaeroides* R-26. I. Protonation of the one-electron states $D^+Q_A^-$, $DQ_A^-$, $D_AQ_AQ_B^-$, and $DQ_AQ_B^-$, *Biochim. Biophys. Acta 934*, 348−368.
89. McPherson, P. H., Schonfeld, M., Paddock, M. L., Okamura, M. Y., and Feher, G. (1994) Protonation and free energy changes associated with formation of $Q_BH_2$ in native and Glu-L212 → Gln mutant reaction centers from *Rhodobacter sphaeroides*, *Biochemistry 33*, 1181−1193.
90. Graige, M. S., Paddock, M. L., Feher, G., and Okamura, M. Y. (1999) Observation of the protonated semiquinone intermediate in isolated reaction centers from *Rhodobacter sphaeroides*: Implications for the mechanism of electron and proton transfer in proteins, *Biochemistry 38*, 11465−11473.
91. Rabenstein, B., Ullmann, G. M., and Knapp, E.-W. (1998) Calculation of protonation patterns in proteins with structural relaxation and molecular ensembles-application to the photosynthetic reaction center, *Eur. Biophys. J. 27*, 626−637.
92. McPherson, P. H., Okamura, M. Y., and Feher, G. (1993) Light-induced proton uptake by photosynthetic reaction centers from *Rhodobacter sphaeroides* R-26.1. II. Protonation of the state $DQ_AQ_B^{2-}$, *Biochim. Biophys. Acta 1144*, 309−324.
93. Kleinfeld, D., Okamura, M. Y., and Feher, G. (1985) Electron transfer in reaction centers of *Rhodopseudomonas sphaeroides*. II. Free energy and kinetic relations between the acceptor states $Q_A^-Q_B^-$ and $Q_AQ_B^{2-}$, *Biochim. Biophys. Acta 809*, 291−310.
94. Ermler, U., Fritzsch, G., Buchanan, S. K., and Michel, H. (1994) Structure of the photosynthetic reaction centre from *Rhodobacter sphaeroides* at 2.65 Å resolution: Cofactors and protein−cofactor interactions, *Structure 2*, 925−936.
95. Fyfe, P. K., and Jones, M. R. (2000) Re-emerging structures: Continuing crystallography of the bacterial reaction centre, *Biochim. Biophys. Acta 1459*, 413−421.
96. Kirmaier, C., Holten, D., and Parson, W. W. (1985) Temperature and detection-wavelenth dependence of the picosecond electron-transfer kinetics measured in *Rhodopseudomonas sphaeroides* reaction centers. Resolution of new spectral and kinetic compon-

tents in the primary charge separation process, *Biochim. Biophys. Acta 810*, 33−48.
97. Li, J., Gilroy, D., Tiede, D. M., and Gunner, M. R. (1998) Kinetic phases in the electron transfer from $P^+Q_A^-Q_B$ to $P^+Q_AQ_B^-$ and the associated processes in *Rhodobacter sphaeroides* R-26 reaction centers, *Biochemistry 37*, 2818−2829.
98. Warncke, K., and Dutton, P. L. (1993) Experimental resolution of the free energies of aqueous solvation contributions to ligand-protein binding: Quinone-$Q_A$ site interactions in the photosynthetic reaction center protein, *Proc. Natl. Acad. Sci. U.S.A. 90*, 2920−2924.
99. McComb, J. C., Stein, R. R., and Wraight, C. A. (1990) Investigations on the influence of headgroup substitution and isoprene side-chain length in the function of primary and secondary quinones of bacterial reaction centers, *Biochim. Biophys. Acta 1015*, 156−171.
100. Paddock, M. L., Graige, M. S., Feher, G., and Okamura, M. Y. (1999) Identification of the proton pathway in bacterial reactions centers: Inhibition of proton transfer by binding of $Zn^{2+}$ or $Cd^{2+}$, *Proc. Natl. Acad. Sci. U.S.A. 96*, 6183−6188.
101. Graige, M. S., Feher, G., and Okamura, M. Y. (1998) Conformational gating of the electron-transfer reaction $Q_A^-Q_B \rightarrow Q_AQ_B^-$ in bacterial reaction centers of *Rhodobacter sphaeroides* determined by a driving force assay, *Proc. Natl. Acad. Sci. U.S.A. 95*, 11679−11684.
102. Kuglstatter, A., Ermler, U., Michel, H., Baciou, L., and Fritzsch, G. (2001) X-ray structure analyses of photosynthetic reaction center variants from *Rhodobacter sphaeroides*: Structural changes induced by point mutations at position L209 modulate electron and proton transfer, *Biochemistry 40*, 4253−4260.
103. Baxter, R. H. G., Ponomarenko, N., Srajer, V., Pahl, R., Moffat, K., and Norris, J. R. (2004) Time-resolved crystallographic studies of light-induced structural changes in the photosynthetic reaction centers, *Proc. Natl. Acad. Sci. U.S.A. 101*, 5982−5987.
104. Nabedryk, E., Breton, J., Joshi, H. M., and Hanson, D. K. (2000) Fourier transform infrared evidence of proton uptake by glutamate L212 upon reduction of the secondary quinone ($Q_B$) in the photosynthetic reaction center from *Rhodobacter capsulatus*, *Biochemistry 39*, 14654−14663.
105. Mezzetti, A., Nabedryk, E., Breton, J., Okamura, M. Y., Paddock, M. L., Giacometti, G., and Leibl, W. (2002) Rapid-scan Fourier transform infrared spectroscopy shows coupling of GLu-L212 protonation and electron transfer to $Q_B$ in *Rhodobacter sphaeroides* reaction centers, *Biochim. Biophys. Acta 1553*, 320−330.
106. Camara-Artigas, A., Brune, D., and Allen, J. P. (2002) Interactions between lipids and bacterial reaction centers determined by protein crystallography, *Proc. Natl. Acad. Sci. U.S.A. 99*, 11055−11060.
107. Lavergne, J., Matthews, C., and Ginet, N. (1999) Electron and proton transfer on the acceptor side of the reaction center in chromatophores of *Rhodobacter capsulatus*: Evidence for direct protonation of the semiquinone state of $Q_B$, *Biochemistry 38*, 4542−4552.
108. Gunner, M. R., Nicholls, A., and Honig, B. (1996) Electrostatic potentials in *Rhodopseudomonas viridis* reaction center: Implications for the driving force and directionality of electron transfer, *J. Phys. Chem. 100*, 4277−4291.
109. Rinyu, L., Martin, E. W., Takahashi, E., Maroti, P., and Wraight, C. A. (2004) Modulation of the free energy of the primary quinone acceptor $Q_A$ in reaction centers from *Rhodobacter sphaeroides*: Contributions from the protein and protein−lipid(cardiolipin) interactions, *Biochim. Biophys. Acta 1655*, 93−101.
110. Ginet, N., and Lavergne, J. (2000) Interactions between the donor and acceptor sides in bacterial reaction centers, *Biochemistry 39*, 16252−16262.
111. Kleinfeld, D., Abresch, E. C., Okamura, M. Y., and Feher, G. (1984) Damping of oscillations in the semiquinone absorption in reaction centers after successive flashes: Determination of the equilibrium between $Q_A^-Q_B$ and $Q_AQ_B^-$, *Biochim. Biophys. Acta 765*, 406−409.
112. Gunner, M. R., and Zhu, Z. (2004) Protons forge new paths, *Structure 12*, 518−519.
113. Xu, Q., Axelrod, H. L., Abresch, E. C., Paddock, M. L., Okamura, M. Y., and Feher, G. (2004) X-ray structure determination of three mutants of the bacterial photosynthetic reaction centers from *Rhodobacter sphaeroides*: Altered proton-transfer pathways, *Structure 12*, 703−715.

BI048348K